

To appear in the *Astrophysical Journal*.

## An Ultra-High-Resolution Survey of the Interstellar ${}^7\text{Li}$ -to- ${}^6\text{Li}$ Isotope Ratio in the Solar Neighborhood

David C. Knauth<sup>1,2,3</sup>, S. R. Federman<sup>1,3</sup>, and David L. Lambert<sup>4</sup>

### ABSTRACT

In an effort to probe the extent of variations in the interstellar  ${}^7\text{Li}/{}^6\text{Li}$  ratio seen previously, ultra-high-resolution ( $R \sim 360,000$ ), high signal-to-noise spectra of stars in the Perseus OB2 and Scorpius OB2 Associations were obtained. These measurements confirm our earlier findings of an interstellar  ${}^7\text{Li}/{}^6\text{Li}$  ratio of about 2 toward  $\sigma$  Per, the value predicted from models of Galactic cosmic ray spallation reactions. Observations of other nearby stars yield limits consistent with the isotopic ratio  $\sim 12$  seen in carbonaceous chondrite meteorites. If this ratio originally represented the gas toward  $\sigma$  Per, then to decrease the original isotope ratio to its current value an order of magnitude increase in the Li abundance is expected, but is not seen. The elemental K/Li ratio is not unusual, although Li and K are formed via different nucleosynthetic pathways. Several proposals to account for the low  ${}^7\text{Li}/{}^6\text{Li}$  ratio were considered, but none seems satisfactory.

Analysis of the Li and K abundances from our survey highlighted two sight lines where depletion effects are prevalent. There is evidence for enhanced depletion toward X Per, since both abundances are lower by a factor of 4 when compared to other sight lines. Moreover, a smaller Li/H abundance is observed toward 20 Aql, but the K/H abundance is normal, suggesting enhanced Li depletion (relative to K) in this direction. Our results suggest that the  ${}^7\text{Li}/{}^6\text{Li}$  ratio has not changed significantly during the last 4.5 billion years and that a ratio  $\sim 12$  represents most gas in the solar neighborhood. In addition, there appears to be a constant stellar contribution of  ${}^7\text{Li}$ , indicating that one or two processes dominate its production in the Galaxy.

---

<sup>1</sup>Department of Physics and Astronomy, University of Toledo, 2801 W. Bancroft, Toledo, OH 43606; sfederm@uoft02.utoledo.edu.

<sup>2</sup>Current address: *FUSE* Science Center, Department of Physics and Astronomy, The Johns Hopkins University, 3400 N. Charles St. Baltimore, MD 21218; dknauth@pha.jhu.edu.

<sup>3</sup>Guest Observer, McDonald Observatory, University of Texas at Austin.

<sup>4</sup>Department of Astronomy, University of Texas at Austin, Austin, TX 78712; dll@astro.as.utexas.edu.

*Subject headings:* ISM: atoms – ISM: abundances – Galaxy: open clusters and associations: individual (Per OB2, Sco OB2) – Galaxy: solar neighborhood – Stars: individual (*o* Per, X Per,  $\chi$  Oph,  $\zeta$  Oph, and 20 Aquilae)

## 1. Introduction

One of the primary goals in astronomy centers on the origin of the elements, but a complete picture remains elusive. Our focus is an improved understanding of light element synthesis through observations of interstellar lithium in diffuse clouds. Since models of Big Bang nucleosynthesis (BBN) yield 10% of the current abundance of  ${}^7\text{Li}$  and negligible amounts of  ${}^6\text{Li}$  (Suzuki, Yoshi, & Beers 2000), much theoretical effort has gone into finding the source for Li. In the 1970's, the work of Reeves and collaborators (Reeves, Fowler, & Hoyle 1970; Meneguzzi, Audouze, & Reeves 1971, hereafter (MAR); Reeves et al. 1973; Reeves 1974) provided an alternate method of light element production which plays an important role throughout the history of the Galaxy. This process is now known as standard Galactic cosmic ray (GCR) spallation. Light elements are created when interstellar C, N, and O nuclei are broken apart by Galactic cosmic rays, the spallation process, and by  $\alpha - \alpha$  fusion reactions. The exact nature of the cosmic ray source is still under debate (e.g., Ramaty et al. 2000a; Fields et al. 2001). Two commonly accepted creation mechanisms for cosmic rays involve supernovae; p and  $\alpha$  particles are produced in and then accelerated by the explosion or are sputtered off interstellar grains and then accelerated.

A low energy cosmic ray (LECR) component, accelerated C and O nuclei, may also be present (Ramaty, Kozlovsky, & Lingenfelter 1996). Lithium, beryllium, and boron are produced through the inflight fragmentation of C and O nuclei during collisions with ambient interstellar H and He (Cassé, Lehoucq, Vangioni-Flam 1995; Higdon, Lingenfelter, & Ramaty 1998; Lemoine, Vangioni-Flam, & Cassé 1998; Lingenfelter, Ramaty, & Kozlovsky 1998; Vangioni-Flam et al. 1998; Parizot & Drury 1999; Ramaty & Lingenfelter 1999; Vangioni-Flam, Cassé, & Audouze 2000). The inverse of standard GCR reactions, this LECR component originates from core collapse supernovae (SN II) grouped in a superbubble (Higdon et al. 1998; Lingenfelter et al. 1998). Both standard GCR and LECR/superbubble models are able to account for the present day abundance of  ${}^6\text{Li}$ ,  ${}^9\text{Be}$ , and  ${}^{10}\text{B}$ , but only 10 – 25% of  ${}^7\text{Li}$  and about 50% of  ${}^{11}\text{B}$  (e.g. MAR; Ramaty et al. 1997).

The rapid rise in the  ${}^7\text{Li}$  abundance for stars with  $[\text{Fe}/\text{H}] \geq -0.5$  indicates the existence of a stellar source of  ${}^7\text{Li}$ . Proposed stellar sources include asymptotic giant branch (AGB; Smith & Lambert 1989, 1990; Plez, Smith, & Lambert 1993) and red giant branch (RGB; Smith et al. 1995) stars, with contributions from SN II and possibly novae. In AGB and RGB

stars rapid transport of  ${}^7\text{Be}$  (Cameron & Fowler 1971; Boothroyd, Sackmann, & Wasserburg 1994, 1995; Wasserburg, Boothroyd, Sackmann 1995) between the He burning shell and the envelope yields  ${}^7\text{Li}$ . In Type II supernovae (SN II), the flux of neutrinos becomes so great that the spallation of heavy nuclei, C, N, and O, into light elements can occur. Through spallation in the He and C shells, SN II can produce observable amounts of both  ${}^7\text{Li}$  and  ${}^{11}\text{B}$  (Woosley et al. 1990; Woosley & Weaver 1995). Another possible thermonuclear source of  ${}^7\text{Li}$  is novae. Novae are predicted to play a significant part in the  ${}^7\text{Li}$  abundance (Starrfield et al. 1978; Romano et al. 2001). The nature of the processes involved in the production of  ${}^7\text{Li}$  is still unclear. A goal of our survey of the interstellar  ${}^7\text{Li}/{}^6\text{Li}$  ratio is to shed light on the importance of the various processes.

Interstellar Li was first detected in the early 1970’s (Traub & Carleton 1973). Since then there have been relatively few reported observations of interstellar Li I. The early detections (Traub & Carleton 1973; Vanden Bout et al. 1978; Snell & Vanden Bout 1981; Hobbs 1984; White 1986) showed weak interstellar Li I absorption, barely discernible from the noise, with equivalent widths ( $W_{\lambda s}$ ) on the order of at most a few mÅ. These early observations showed that the interstellar Li I abundance was similar along different lines of sight. However, large uncertainties remained due to low signal-to-noise ratios and uncertain corrections for ionization and depletion onto grains. With the advent of modern detectors and more sophisticated observing techniques, reliable observations of  ${}^7\text{Li}$ , and the much weaker  ${}^6\text{Li}$  line, were possible (Ferlet & Dennefeld 1984; Lemoine et al. 1993; Lemoine, Ferlet, & Vidal-Madjar 1995; Meyer, Hawkins, & Wright 1993; Knauth et al. 2000, Howarth et al. 2002).

The Li isotope ratio is crucial for studies of Galactic chemical evolution (Reeves 1993; Steigman 1993) since it is free from uncertain corrections (e.g., ionization and depletion). Published  ${}^7\text{Li}/{}^6\text{Li}$  ratios in the local ISM indicate that the ratio may vary from the Solar System value of 12.3 (Anders & Grevesse 1989), but the results are far from conclusive. Four different isotope ratios have been published for the line of sight toward  $\zeta$  Oph:  $\geq 25$  (Ferlet & Dennefeld 1984) and  $6.8_{-1.7}^{+1.4}$  for a single component fit to the data (Meyer et al. 1993), Lemoine et al. (1995) obtained  $1.4_{-0.5}^{+1.2}$  ( $\pm 0.6$ ) and  $8.6 \pm 0.8$  ( $\pm 1.4$ ) and Howarth et al. (2002) reported an average  ${}^7\text{Li}/{}^6\text{Li}$  ratio of  $13.2 \pm 6.3$  for their two component fit. Lemoine et al. (1993) found an isotope ratio of  $12.5_{-3.4}^{+4.3}$  toward  $\rho$  Oph, consistent with the Solar System value. Knauth et al. (2000) derived isotope ratios for two velocity components toward  $o$  Per of  $1.7 \pm 0.3$  and  $3.6 \pm 0.6$  and an isotope ratio of  $10.6 \pm 2.9$  for a single component toward  $\zeta$  Per. The latter ratio is marginally consistent with the value of  $5.5_{-1.1}^{+1.3}$  reported by Meyer et al. (1993). As discussed in §2, an accurate template for the velocity components along a given sight line appears to be required before consistent results emerge.

In our earlier study (Knauth et al. 2000), high-resolution ( $R \sim 180,000$ ) spectra were obtained on the stars  $\sigma$  and  $\zeta$  Per in the Perseus OB2 Association. These stars were chosen for their proximity to IC 348, an active star-forming region. These data showed that the  ${}^7\text{Li}/{}^6\text{Li}$  ratio varies from the Solar System value toward  $\zeta$  Per to a value of approximately 2 toward  $\sigma$  Per.  $\sigma$  Per resides closer to IC 348 than does  $\zeta$  Per and has an order of magnitude higher flux of cosmic rays (Federman, Weber, & Lambert 1996). Knauth et al. (2000) suggested that the ratio of 2 was clear evidence for newly synthesized lithium toward  $\sigma$  Per resulting from GCR spallation reactions. These data barely resolve the 2 velocity components separated by  $\sim 3 \text{ km s}^{-1}$  toward  $\sigma$  Per. To refine these findings and to probe directions with interstellar clouds separated by  $\sim 1 \text{ km s}^{-1}$ , we obtained ultra-high-resolution (UHR) observations toward other stars in the Perseus OB2 and Scorpius OB2 Associations. The stars in Sco OB2 lie close to an active star-forming region approximately centered on  $\rho$  Oph. Furthermore,  $\lambda$  Ori was observed because it resides in a region of active star formation. In addition, an UHR survey of interstellar K I (Welty & Hobbs 2001) indicated that Li I could possibly be detected toward  $\lambda$  Ori. 20 Aql lies relatively far from active regions of star formation and serves as a useful comparison.

The main goals of the present study were to determine reliable  ${}^7\text{Li}/{}^6\text{Li}$  isotope ratios in order to probe the extent of variations in its value and to help constrain the roots of Li production. Since  ${}^6\text{Li}$  is produced primarily through GCR spallation reactions, the GCR contribution to  ${}^7\text{Li}$  can be accurately determined. Assuming that the BBN contribution is known from observations of halo stars, the remaining  ${}^7\text{Li}$  comes from Population I stars. These assumptions enabled interstellar constraints to be placed on the stellar production of  ${}^7\text{Li}$ . The organization of this paper is as follows. In §2 we describe the observations and the data reduction. The profile syntheses for all data sets are discussed and the results are tabulated in §3. The isotope ratios, Li I and K I column densities, elemental abundances, depletion, and elemental K/Li ratios for each sight line are given in §4. In §5 we discuss implications for future Li studies and thermal vs. turbulent broadening. The results of the  ${}^7\text{Li}/{}^6\text{Li}$  isotope ratios are discussed in §6 and §7. In §8 constraints on stellar sources of  ${}^7\text{Li}$  are presented. Finally, the results are summarized and suggestions for future work are contained in §9.

## 2. Observations and Data Reduction

High signal-to-noise, high-resolution spectra of the Li I doublet are needed, since coupled to the relatively weak absorption, the fine structure separation of the  ${}^7\text{Li}$  I doublet ( $3p \text{ } {}^2P_{3/2, 1/2} - 2s \text{ } {}^2S_{1/2}$  at  $6707.764 \text{ \AA}$  for  $J = 3/2$  and at  $6707.915 \text{ \AA}$  for  $J = 1/2$ ) is com-

parable to the isotope shift of  ${}^6\text{Li}$  ( $\sim 0.160 \text{ \AA}$ ). The result is a blend of the  ${}^7\text{Li}$  and  ${}^6\text{Li}$  lines (Ferlet & Dennefeld 1984; Sansonetti et al. 1995). The situation is further complicated by the existence of several interstellar clouds along the line of sight (typically 6 clouds per kpc). For this reason, UHR surveys [resolving power (R)  $\sim 600,000$ ] of K I (Hobbs 1974a, 1974b; Welty & Hobbs 2001) were used to find lines of sight with simple velocity structure (that is, one or two components) with significant amounts ( $N(\text{K I}) \sim 10^{11} \text{ cm}^{-2}$ ) of absorption. Assuming a constant K/Li ratio (White 1986; Welty & Hobbs 2001), these surveys yielded lines of sight to pursue in the quest for interstellar Li I absorption. Table 1 gives the stellar data for the objects studied here.

In order to extract the interstellar  ${}^7\text{Li}/{}^6\text{Li}$  ratio, knowledge about the velocity structure for a given line of sight (LOS) is necessary. Data on another species are required for use as a template of the velocity structure (Lemoine et al. 1993, 1995; Lambert et al. 1998; Knauth et al. 2000, Howarth et al. 2002). We chose K I because it has a similar ionization potential and is likely to reside in the portion of the interstellar cloud containing Li I (White 1986; Welty & Hobbs 2001). The method used here differs from that of Lemoine et al. (1993, 1995) who adopted K I  $\lambda 7699$  as their velocity template. Instead, K I  $\lambda 4044$  was chosen since it is of comparable strength to the Li I lines, although  $\lambda 7699$  is still useful in revealing weaker structure that may be visible within the  $\lambda 4044$  line profile. Table 2 lists the ionization potential, IP, (Morton 1991), laboratory wavelengths for Li I and K I (Morton 1991; Sansonetti et al. 1995), and the oscillator strengths for Li I and K I fine structure lines (Morton 1991) used in this study. The oscillator strengths for the Li I hyperfine transitions were extracted from the fine structure oscillator strengths (e.g., Welty, Hobbs, & Kulkarni 1994). The hyperfine structure of K I  $\lambda 4044$  was found to be negligible ( $\sim 0.002 \text{ m\AA}$ ).

## 2.1. Ultra-High-Resolution Observations

### 2.1.1. McDonald Observatory

All observations were taken with the double-pass spectrograph of the 6-foot camera on the 2.7 m Harlan J. Smith Telescope at the University of Texas McDonald Observatory. Two spectral regions were observed, one centered on K I  $\lambda 4044$  and the other on Li I  $\lambda 6708$ . The former setting allowed a wavelength coverage of approximately  $1.5 \text{ \AA}$ , while the latter yielded  $2.5 \text{ \AA}$  of spectrum. Since such a narrow wavelength range was imaged, care was needed to ensure that interstellar features with large Doppler motions with respect to the Earth remained within the range of the detector. For this purpose, hollow cathode lamps containing Th-Ar and Li, as well as the solar spectrum, were utilized to determine the spectrograph settings. Only a single weak, uncataloged line appeared in the Th-Ar spectrum

at  $\lambda 6708$ . Therefore, a Li hollow cathode was used for wavelength calibration, even though the pressure broadened Li lines could not be used to determine the instrumental width. An echelle grating was combined with a cross disperser, which was used in  $2^{nd}$  order for the blue setting and in  $1^{st}$  order for the red one. A  $\text{CuSO}_4$  (RG610) blocking filter for the blue (red) setting was placed behind the slit of the spectrograph to isolate the light from a specific order. A slit width of  $145 \mu\text{m}$  (slit #2) was used. The echelle grating position was moved each night to minimize the effects of cosmic rays as well as any flat field artifacts, in hindsight a very wise decision. Stellar exposures of  $30^m$  or less also minimized the confusion caused by cosmic rays. For many of the observing runs, a stellar flat from a bright star was obtained. Unfortunately, due to poor weather conditions, a stellar flat was not obtained for every observing run. This combination of procedures enabled the detection of 1% CCD defects and minimized their effect on the data.

The resolution was determined in the course of the analysis by the full width at half maximum (FWHM) of the Th line at  $4043.395 \text{ \AA}$ . The FWHM was determined to be  $0.01172 \text{ \AA}$  with 7 pixels per resolution element at this wavelength setting. While a lithium hollow cathode provided the wavelength calibration for the  $6708 \text{ \AA}$  region, the lithium lines are dominated by pressure broadening (FWHM  $\approx 0.0425 \text{ \AA}$ ). Since the same spectrograph was utilized for both sets of observations and the resolution is expected to be independent of the wavelength region, the resolution determined from the K I setting was used for the Li I setting. At this resolution, the effects of thermal gas motions must be considered in determining an accurate instrumental width. After correcting for thermal broadening at an assumed temperature of 300 K, the instrumental width was found to be  $0.833 \text{ km s}^{-1}$ , which corresponds to an R of 360,000. This resolution was chosen to discern interstellar clouds separated by  $\approx 1 \text{ km s}^{-1}$ .

The reddened stars,  $\sigma$  Per, 40 Per, X Per,  $\zeta$  Oph, and  $\chi$  Oph, in the Perseus OB2 and Scorpius OB2 Associations were observed, as were  $\lambda$  Ori and 20 Aql. Data were also acquired on the bright unreddened stars  $\gamma$  Cas,  $\alpha$  Leo, and  $\alpha$  Vir. All the observations were obtained over eight observing runs between August 1998 and December 2000. Table 3 contains the following information for each observing run: the stars and species observed, the observatory, the dates of the observing run, the total exposure time for all observations, and the signal-to-noise ratio (SNR) per pixel. Also noted in Table 3 are the SNR per resolution element of the final summed spectra for all stars.

### 2.1.2. *Anglo-Australian Observatory*

Additional data on Li I and the strong K I line at 7699 Å were obtained (Lemoine 1995) from the Anglo-Australian Observatory (AAO) archive. Li I and K I were observed toward the stars,  $\chi$  and  $\zeta$  Oph, while only K I was observed toward the stars,  $o$  Sco,  $\rho$  Oph, HD 154090, HD 165024, and  $\mu$  Sgr. A synopsis also appears in Table 3.

The K I data were reduced to verify the accuracy of our Li I data reduction. Comparison of the measured values of  $W_\lambda$  for K I  $\lambda$ 7699 with those presented in Welty & Hobbs (2001), based on the same data, show excellent agreement with the exception of the absorption toward  $o$  Sco and HD 154090, which differ by approximately 10%. This overall agreement lends confidence that our lithium measurements toward  $\chi$  and  $\zeta$  Oph are reliable.

## 2.2. Standard Data Reduction

The data were reduced in a standard way utilizing the **NOAO SUN/IRAF** software (Revision 2.11.3). Dark, bias, and flat lamp exposures were taken each night to remove any instrumental effects due to the CCD detector. Comparison spectra were taken periodically throughout the night, typically every two hours. The average bias exposure was subtracted from all raw stellar, comparison (Th-Ar), and flat images. The scattered light was fit by a low order polynomial, in both the dispersion direction and perpendicular to it for the multi-order observations, and removed. The pixel-to-pixel sensitivity was taken into account by dividing the normalized flat into the stellar spectra. The normalized flat is the average of 10 – 20 flat lamp (5 – 10 stellar flat) exposures, with each exposure having a flux level 3 – 5 times that of a single stellar exposure. Next, the pixels perpendicular to the dispersion were summed in each order for each stellar and comparison lamp exposure. The extracted spectra were placed on an appropriate wavelength scale using the Th-Ar or Li comparison spectra, and Doppler-corrected. The spectra were then coadded and normalized to unity with a low order polynomial, yielding a final spectrum with high signal to noise (based on the root-mean-square of the deviations in the continuum), approximately 1000:1 per resolution element. Over the narrow wavelength range covered by these spectra, there were at most slight variations in the continua.

Each stellar spectrum was carefully examined for flat field artifacts or cosmic rays before the final spectrum was created. Cosmic rays that survived the reduction were removed. When the cosmic rays coincided with the interstellar features in a spectrum, as was the case with 3 exposures of  $\zeta$  Oph, 2 exposures of 20 Aql and 1 exposure of  $o$  Per, the affected spectra were not included in the final sum. The standard reduction process was successful in

extracting the data for most of the observing runs. While examining the spectra for cosmic rays, the presence of two 1% features (CCD defects) that were not removed during the flat fielding process were detected. An improved flat fielding technique using stellar spectra was applied before the remaining steps in the extraction process.

The defects were seen in all spectra, but for  $\sim 60\%$  of the observing runs the defects were far ( $\sim 200$  pixels) from where the interstellar line(s) appeared. The defects were a problem for the McDonald observing runs of August 1998, December 1999, and December 2000. The basic solution followed the prescription for removal of fixed pattern noise in spectra acquired with the Goddard High-Resolution Spectrograph (Cardelli & Ebbets 1994). The spectrum of an unreddened star was used as a template; removal of the defect was accomplished by dividing the affected spectrum by the template in pixel space, since defects remain fixed in pixel space. Multiple observing runs of the interstellar species toward the same star gave an additional check that proved useful in minimizing the effect of the 1% defects. Where other measures exist for comparison (Meyer et al. 1993; Lemoine et al. 1995; Knauth et al 2000; Howarth et al. 2002), there is good to excellent correspondence among spectra. The McDonald spectra were binned by three pixels to increase the SNR, a valid procedure since there are 7 pixels per resolution element, and the AAO data for  $\chi$  and  $\zeta$  Oph were binned to the lower resolution of the McDonald data before combining them.

### 3. Profile Synthesis

Each interstellar line profile yields the number of velocity components, the wavelength at line center,  $\lambda$ , FWHM, and  $W_\lambda$ , for each component. The number of velocity components in the Li spectrum was obtained from a visual examination of the K I spectrum. For symmetric interstellar lines, the determination of the  $W_\lambda$  is accomplished by fitting a Gaussian profile to the interstellar feature for comparison with the results from the profile synthesis. Asymmetric interstellar lines are telltale signs of multiple components along a given line of sight. If more than one component was present, the task of determining  $W_\lambda$  involved simple Gaussian deblending. Unresolved velocity structure is treated as a single component and may result in slight differences in the derived quantities. There are additional uncertainties in the calculated  $V_{LSR}$  ( $\sim 0.5$  km s $^{-1}$ ) derived from the K I and Li I lines. This difference is attributed to the uncertainty in the wavelength calibration for the Li I region, the result of there being larger widths for the pressure broadened, hollow cathode lines of Li I. For the stars,  $\gamma$  Cas,  $\alpha$  Leo, and  $\alpha$  Vir, as well as 40 Per and  $\lambda$  Ori, no detection of Li I or K I was evident. For these stars the 3- $\sigma$  upper limits, determined from the SNR and the FWHM of the instrument function, are listed in Table 4 and will not be discussed further.



Continuum placement uncertainties were not included in the error budget because variation in the continua was found to be insignificant.

If a single velocity component is present along a given sight line, then a simple Gaussian can be fitted to the line profile in order to determine these three parameters. A more realistic approximation of the profile function is given by a Voigt profile. While a Voigt profile more precisely describes the wings of saturated absorption lines, Gaussian profiles were adequate in fitting the weak Li I and K I lines observed in this study. If multiple components are present, the determination of  $b$ -value,  $V_{LSR}$ , and  $N$  is more complicated.

A C++ code (J. Zsargó 2000, private communication) was utilized to compare the observed K I and Li I line profiles with synthetic ones. The two profiles were synthesized independently. Comparison of observed and synthetic profiles was performed with a second-order gradient-expansion Marquardt algorithm (Bevington & Robinson 1992). The synthetic profiles and  $\chi^2$  were calculated with initial values of the parameters. The gradient-expansion method adjusts the initial values and the process is repeated with the updated values until a change in  $\chi^2$  of less than 0.01% occurs. An additional feature of the program allowed any parameter to be fixed in order to arrive at a solution. One or more parameters were fixed only when a high degree of certainty in the initial parameters was present. For details of the profile synthesis see Zsargó & Federman (2002).

Reliable initial values are crucial to finding the most appropriate minima since there could be several minima caused by multiple velocity components or lower SNR. The syntheses gave the  $b$ -value,  $V_{LSR}$ , and  $N$  for each component as well as the total  $W_\lambda$ . Agreement between the observed  $W_\lambda$  and that from the combination of the components was at the  $1\text{-}\sigma$  level, with the exception of the  $7\text{ km s}^{-1}$  component toward  $o$  Per (see §3.2). The best fit was inferred from F-tests for trials based on fits using different numbers of components. Figures 1 – 5 shows our UHR spectra obtained toward  $o$  Per, X Per,  $\chi$  Oph,  $\zeta$  Oph, and 20 Aql, respectively. From a visual examination of our spectra, only the clouds toward  $o$  Per reveal large  ${}^6\text{Li}$  abundances – compare Figures 1 – 5. Profile synthesis provides a quantitative isotope ratio in all cases. In addition, the enhanced  ${}^6\text{Li}$  abundance toward  $o$  Per is clearly seen in our lower resolution spectrum (Knauth et al. 2000).

### 3.1. $o$ Per

At our resolution, a very weak absorption line provided by a single cloud of pure  ${}^7\text{Li}$  would be seen as a resolved doublet with the ‘blue’ line twice the depth of the ‘red’ line. Addition of  ${}^6\text{Li}$  increases the depth of the ‘red’ line which reduces the blue-to-red ratio of

line depths below the 2 to 1 ratio set by atomic physics (i.e., LS coupling). Superficial inspection of the profiles at the telescope showed that all lines of sight but one were at or close to this 2 to 1 ratio. The exception was *o* Per where the ‘red’ line appeared deeper than expected (Figure 1), a telltale signature that either a high  ${}^6\text{Li}$  abundance in the cloud or the presence of a second higher velocity cloud contributing  ${}^7\text{Li}$  at about  $+7\text{ km s}^{-1}$  from the main cloud could be masquerading as  ${}^6\text{Li}$ ;  $+7\text{ km s}^{-1}$  is the isotopic shift. The weaker  ${}^6\text{Li}$  line, which is about  $0.16\text{ \AA}$  to the red of the weaker  ${}^7\text{Li}$  line, would be of value in determining the reason for the deeper ‘red’ line, but, unfortunately, the line is indistinguishable from the noise of the spectrum - see also the lower resolution spectra published by Knauth et al. (2000). Figure 6 shows our previous high-resolution Li I spectrum (Knauth et al. 2000), fit with a synthetic spectrum assuming a Solar System isotope ratio of 12 for both velocity components. Examination of Figure 6 clearly shows an enhanced  ${}^6\text{Li}$  abundance.

Our template K I 4044  $\text{\AA}$  profiles and those provided by observations of the K I 7699  $\text{\AA}$  line (Welty & Hobbs 2001) serve to constrain the distribution of clouds toward *o* Per. Our 4044  $\text{\AA}$  spectrum shows two clouds separated by about  $3\text{ km s}^{-1}$  and both clouds are seen to contribute to the Li I profile (Figure 1). Welty and Hobbs’s higher resolution observations of the 7699  $\text{\AA}$  K I line show that each of our clouds is a pair of clouds with a velocity separation of  $1.0\text{ km s}^{-1}$  for the weaker cloud and  $1.3\text{ km s}^{-1}$  for the stronger cloud. A fifth cloud, at a velocity of about  $2\text{ km s}^{-1}$  to the red of the stronger line in Figure 1, has a column density of only 6% of that in the stronger cloud. This fifth component is hidden by the noise in Figure 1.

Independent analyses of the Li I and K I profiles began with the introduction of the two velocity components clearly detected in Figure 1. The reduced- $\chi^2$  ( $\chi^2/\nu$ ) of both fits (Figure 1) are at the 90 - 95% confidence level. Derived parameters from these independent fits are given in Table 5. Considering the accuracy of the velocity scales, the small difference in the cloud velocities derived from the K I and Li I syntheses is not significant. As can be seen in Figure 6, a Solar System ratio for both velocity components yields a poor fit to the data. A fit to the Li I absorption was also made using the  $V_{LSR}$  and  $b$ -values from the K I synthesis (see bottom panel of Figure 1). Although the isotopic ratios are altered slightly, the quality of this fit is poor ( $\chi^2/\nu = 3.73$ ) on account of the smaller  $b$ -values for K I. This suggests (see below) that thermal broadening is the main contributor to the  $b$ -values.

Our earlier spectra of the K I and Li I absorption were acquired at a factor of 2 lower resolution and with a signal to noise ratio of 2500:1. A two-cloud analysis gave isotopic ratios of  $1.7 \pm 0.3$  and  $3.6 \pm 0.6$  for the 4 and 7  $\text{km s}^{-1}$  clouds, respectively (Knauth et al. 2000). Our result, for the 4  $\text{km s}^{-1}$  component, of  $2.1 \pm 1.1$  confirms the earlier result, but our current result of  $8.1 \pm 2.1$  is in poor agreement with the earlier result. The measured  $W_{\lambda s}$

for the blue component of  ${}^7\text{Li I}$  and both components of  $\text{K I}$  agree well with our previous measurements (Knauth et al. 2000). However, the red component in  $\text{Li}$  is  $0.1 \text{ m}\text{\AA}$  larger than that obtained in Knauth et al. (2000). The larger  $W_\lambda$  could be due to an undetected CCD defect. Therefore, the profile synthesis of the UHR data was also performed utilizing the results of Knauth et al. (2000). This synthesis resulted in a reasonable fit to the data. Although both syntheses are equally acceptable, the resulting column densities only overlap at the  $3\text{-}\sigma$  level, suggesting that the observational errors alone are inadequate in representing the true uncertainty. A Solar System isotope ratio for both components is unlikely due to the almost one-to-one correspondence between both members of the  $\text{Li I}$  doublet (see Figure 6).

As noted above, our  $\text{K I}$  components are each a blend of two close components. If these four clouds are included instead of two, constrained fits are possible using the  $b$ -values from Welty & Hobbs (2001), although the isotopic ratios are not changed significantly. Three component syntheses of the  $\text{K I}$  and  $\text{Li I}$  line profiles resulted in an increased  $\chi^2/\nu$  (1.51 for  $\text{K I}$  and 3.32 for  $\text{Li I}$ ) when compared to the two component syntheses. Application of an F test (Lupton 1993) shows that a third component is justified at the 70% confidence level, while a fourth component yields only a 50% confidence. In order to investigate the possibility of  ${}^7\text{Li}$  masquerading as  ${}^6\text{Li}$ , another synthesis was performed that incorporated the reddest component from Welty & Hobbs (2001). This additional component was found to be indistinguishable from the noise in the  $4044 \text{ \AA}$  line profile. Again the quality of the fit is poor and does not change the occurrence of the low  $\text{Li}$  isotope ratio.

An additional probe of cloud structure along the line of sight is provided by the  $\text{Na D}$  profile (Welty & Hobbs 2001), a more sensitive monitor of thin clouds than the  $7699 \text{ \AA}$  line. Four additional clouds are seen in  $\text{Na D}$ : two to the red of the stronger  $\text{K I}$  line in Figure 1 and two to the blue of the weaker  $\text{K I}$  line.  $\text{Na I}$  column densities in these clouds do not exceed 1% of the observed column in the strongest of the five clouds detected in both  $\text{Na D}$  and  $\text{K I}$ . Of relevance - perhaps - to the  $\text{Li}$  isotopic analysis is that the velocity shifts of additional clouds to the red are approximately equal to the velocity shift of  ${}^6\text{Li}$  from  ${}^7\text{Li}$  in the two main pairs of clouds.

These clouds of low  $\text{Na I}$  column density appear at velocities relative to the main clouds that, if they contributed  ${}^7\text{Li}$  absorption, would reduce and even eliminate the need for  ${}^6\text{Li}$  absorption from the main clouds. Another synthesis resulted in a reasonable fit to the data with limits to the  ${}^7\text{Li}/{}^6\text{Li}$  similar to the Solar System value for all velocity components. In order to achieve this, however, the ratio of  $N(\text{Li I})$  to  $N(\text{Na I})$  for the two reddest clouds must be about  $10^4$  times that in typical clouds (Welty & Hobbs 2001). Unfortunately, this argument replaces one astrophysical puzzle – why is the  ${}^7\text{Li}/{}^6\text{Li}$  ratio so low? – for another – why is the ratio of  $\text{Li}$  to  $\text{Na}$  atoms so high in the higher velocity clouds? Inclusion of these

low column density components into the synthesis adds the additional complication that these components contain little or no K I absorption. It is interesting to note that the higher velocity clouds are seen in both Na I and Ca II toward *o* Per, but only Ca II absorption is detected toward  $\zeta$  Per for which a normal  ${}^7\text{Li}/{}^6\text{Li}$  ratio is found (Knauth et al. 2000). The uncertainties and substitution of one puzzle for another suggest that the best results from the profile synthesis of the *o* Per data are given by the two component fit, indicating that the low relative strengths for the  ${}^7\text{Li}$  doublet are the result of enhanced  ${}^6\text{Li}$  in one or both of the clouds.

### 3.2. Other Sight Lines

The analyses of the other sight lines yielded lower limits to the  ${}^7\text{Li}/{}^6\text{Li}$  ratio consistent with the Solar System value. The weaker  ${}^7\text{Li}$  line was used to constrain the maximum amount of  ${}^6\text{Li}$  present, since this feature is a blend of the  ${}^7\text{Li}$  and  ${}^6\text{Li}$  lines and the ratio of  ${}^7\text{Li}$  is 2 to 1. The profile synthesis produced a formal detection to  $\chi$  Oph which is consistent with these limits. The syntheses for these four sight lines also provided the means to extract the relative importance of thermal and turbulent broadening from the *b*-values of Li and K. We now describe the particulars for each sight line.

*X Per* – At least one velocity component is clearly detected in Li I absorption. Unfortunately, data on K I  $\lambda 4044$  is not available for this sight line, a result of *X Per* being the faintest star studied here. Observations of K I  $\lambda 7699$  reveal more complicated velocity structure (2 components with an  $R \sim 200,000$ , S. R. Federman 2001, private communication; 4 components with an  $R \sim 600,000$ , D. Welty 2001, private communication). All three syntheses yield good fits, with  $\chi^2/\nu$  at the 85 – 95% confidence level. An F test on the data revealed 95% confidence in the 2 component fit and 74% confidence in the 4 component fit. Higher S/N data are necessary to distinguish the most appropriate velocity structure in Li I absorption for this line of sight. The best fit, with two velocity components, is displayed in Figure 2; the results appear in Table 5. The *b*-values,  $1.20 \text{ km s}^{-1}$  and  $1.15 \text{ km s}^{-1}$ , are similar to those derived from K I  $\lambda 7699$  absorption,  $1.7 \text{ km s}^{-1}$  and  $1.2 \text{ km s}^{-1}$  (S. R. Federman 2001, private communication), suggesting that turbulence dominates the interstellar clouds toward *X Per*.

$\chi$  *Oph* – Only one velocity component is present. Multiple velocity components are seen in UHR K I  $\lambda 7699$  spectra (Welty & Hobbs 2001). An unrealistic fit resulted (e.g., an emission line) from a two component synthesis of the K I  $\lambda 4044$  absorption. A significantly weaker third velocity component is at least  $2 \text{ km s}^{-1}$  away (Welty & Hobbs 2001), but is within the noise level in our data. The single component synthesis of the line profiles is shown in

Figure 3. The slight disagreement for the weaker  ${}^7\text{Li}$  line with the results of the synthesis is most likely caused by a CCD defect within the level of noise. The  $\chi^2/\nu$  for the top two fits are at the 90 – 95% confidence level. The results of these independent syntheses are presented in Table 5. The synthesis of Li I with the smaller  $b$ -values derived from the K I fit is not acceptable ( $\chi^2/\nu = 2.06$ ); thermal broadening dominates this interstellar cloud. As a test for a single primary component, a self-consistent  $b$ -value was calculated for K I  $\lambda 7699$  utilizing  $N(\text{K I})$  derived from  $\lambda 4044$  and the total  $W_\lambda$  of the two velocity components of  $\lambda 7699$  (Welty & Hobbs 2001). This results in a  $b = 0.75 \text{ km s}^{-1}$ , which agrees with the  $b$ -value of Welty & Hobbs (2001) within their quoted  $0.1 \text{ km s}^{-1}$  uncertainty.

$\zeta \text{ Oph}$  – Two velocity components, separated by  $\sim 1 \text{ km s}^{-1}$ , are clearly detected in both K I and Li I absorption toward  $\zeta \text{ Oph}$ . Figure 4 shows the results of this two velocity component fit to K I (top panel) and Li I (middle panel). There is also a slight mismatch between the fit and the data in the weaker  ${}^7\text{Li}$  line, which also occurred for  $\chi \text{ Oph}$ , most likely caused by a CCD defect within the level of noise. The results of the two component fit are exceptional for K I and quite good for the Li I absorption, as shown in Table 5. A single component with an equivalent width of  $0.638 \text{ m}\text{\AA}$  was reported toward  $\zeta \text{ Oph}$  by Meyer et al. (1993),  $0.55 \text{ m}\text{\AA}$  for the combined two components by Lemoine et al. (1995), and  $0.68 \text{ m}\text{\AA}$  for the combined two components of Howarth et al. (2002). These measurements agree well with the combined  $W_\lambda$  for the two velocity components,  $0.55 \text{ m}\text{\AA}$ , reported here. The K I parameters fit the Li I profile as well, suggesting that turbulent broadening dominates. UHR data (Welty & Hobbs 2001) show three additional relatively weak K I  $\lambda 7699$  absorption components [ $N(\text{K I}) \sim 1 \times 10^{10} \text{ cm}^{-2}$ ], approximately  $1 \text{ km s}^{-1}$  to longer wavelengths and  $1 \text{ km s}^{-1}$  and  $4 \text{ km s}^{-1}$  to shorter wavelengths than the two stronger components. These relatively weak components are at the level of the noise in our  $\lambda 4044$  spectrum. Inclusion of a third component into our K I and Li I profile syntheses, with the parameters taken from Welty & Hobbs (2001), results in only a 50% confidence in there being another component. Howarth et al. (2002) also find no evidence for a third component.

$20 \text{ Aql}$  – There are two components clearly detected in K I and  ${}^7\text{Li}$  I. Figure 5 shows the fits to both K I and Li I using each species to determine the profile parameters. The results of the independent fits are shown in Table 5. The bottom graph shows the fit to Li I using the parameters derived from the K I synthesis. This fit has a slightly larger reduced  $\chi^2$  (1.36) because the derived  $b$ -values from the Li I fit are slightly larger ( $\sim 0.5 \text{ km s}^{-1}$ ) than the values found from the K I fit, indicating the importance of thermal broadening.

## 4. Analysis

### 4.1. ${}^7\text{Li}/{}^6\text{Li}$ Ratios

The  ${}^7\text{Li}/{}^6\text{Li}$  ratios, a direct result of the profile synthesis, are listed in Table 5. The uncertainties were determined from the weighted average of both the  ${}^7\text{Li}$  and  ${}^6\text{Li}$  column densities (when present). The lower limits are derived from the expected relative line strengths for the  ${}^7\text{Li}$  doublet (2:1). Toward *o* Per, one velocity component is nearly identical to the value predicted by models of GCR spallation reactions ( $\sim 2$ ), while the other component may be similar to the Solar System value of 12.3 (see Knauth et al. 2000) as are the isotope ratios, or their limits, toward X Per,  $\chi$  Oph,  $\zeta$  Oph, and 20 Aql.

Other measures of the isotope ratio are available for comparison. The determination of  ${}^7\text{Li}/{}^6\text{Li} = 5.5_{-1.1}^{+1.3}$  toward  $\zeta$  Per, from spectra with  $R \sim 200,000$  and SNR of 2100, (Meyer et al. 1993) is marginally consistent with our previous observations taken at a similar resolution and with a SNR of 2500 which resulted in a  ${}^7\text{Li}/{}^6\text{Li}$  ratio of  $10.6 \pm 2.9$  (Knauth et al. 2000). Toward  $\rho$  Oph, where a single velocity component is present, a ratio of  $12.5_{-3.4}^{+4.3}$  was reported (Lemoine et al. 1993) from spectra obtained at  $R \sim 100,000$  and SNR of 2700. A single component toward  $\zeta$  Oph yields  ${}^7\text{Li}/{}^6\text{Li} = 6.8_{-1.7}^{+1.4}$  from spectra with  $R \sim 200,000$  and SNR of 2300 (Meyer et al. 1993), but it is actually two velocity components separated by  $1 \text{ km s}^{-1}$  (Lambert, Sheffer, & Crane 1990; Crawford et al. 1994; Crawford & Barlow 1996; Welty & Hobbs 2001; this work). Lemoine et al. (1995) reported isotope ratios of  $1.4_{-0.5}^{+0.8}$  ( $\pm 0.6$ ) and  $8.6 \pm 0.8$  ( $\pm 1.4$ ) for two velocity components separated by  $\sim 5 \text{ km s}^{-1}$  from spectra taken at  $R$  of 100,000 and with a SNR of 7500. The latter is the single component described by Meyer et al. (1993). In a recent paper, Howarth et al. (2002) report an average  ${}^7\text{Li}/{}^6\text{Li}$  ratio of  $13.2 \pm 6.3$  for their two component fit toward  $\zeta$  Oph based on spectra taken at  $R \sim 10^6$  and a signal-to-noise ratio of 1200:1.

Lemoine et al.’s results for the weaker bluer component at  $V_{helio} = -19 \text{ km s}^{-1}$  with the low isotope ratio toward  $\zeta$  Oph raises a number of issues. First, the  ${}^7\text{Li}$  I feature is but a 2 to 3- $\sigma$  detection, and similar positive excursions appear in their spectrum (their Figure 6). Second, this component has a K/Li ratio much smaller than that found here for this sight line and others. Another problem is that there is no molecular material associated with the velocity component having a low isotope ratio. For all other lines of sight in which Li I has been detected, substantial molecular material is found at the velocity of Li I  $\lambda 6707$ . The component may be the result of using the strong K I line at 7699 /AA/ as the velocity template because it detects weaker interstellar features than will be seen in Li I. The weak K I  $\lambda 7699$  component is at the limit of our signal to noise in  $\lambda 4044$ . No evidence for the weak velocity component in Li I toward  $\zeta$  Oph is suggested by our data or that of Howarth

et al. (2002). These facts seem to indicate that a velocity component with a low isotope ratio is not present toward  $\zeta$  Oph. It is important to note that the SNR of Lemoine et al.’s data is a factor of 2 larger than the SNR of our data.

#### 4.2. Neutral Columns of Li and K

Figure 7 shows a comparison of  $N(\text{Li I})$  to  $N(\text{K I})$ . The least squares fit (solid line) for all lines of sight studied here and in Welty & Hobbs (2001) is shown. The dotted line is the best fit from Welty & Hobbs (2001). Our least squares fit includes the uncertainties from this work and Knauth et al. (2000), as well as the observational uncertainties for Li I and an assumed 20% uncertainty in the K I values (Welty & Hobbs 2001 and references therein). Since a fit of data points derived from individual velocity structure (asterisks) has a higher correlation coefficient ( $r=0.92$ ) than does the fit ( $r=0.81$ ) based on total columns (solid circles), use of individual velocity components along the line of sight is the more appropriate means for comparison. Another consideration is that some of the Li I observations from the literature are only modest detections at best; higher quality data may also improve the correlation coefficient. Significantly greater dispersion about our fit arises when alternative component structures discussed in §3 are included; we consider this further evidence for the preferred results given in Table 5.

The furthest data point from the fits is for the LOS toward HD 154368. This LOS has the largest column of Li I reported (Snow et al. 1996), almost an order of magnitude larger than toward  $\rho$  Oph, the next largest reported column density (White 1986; Lemoine et al. 1993; Knauth et al. unpublished). The measurement toward HD 154368 could be as much as a factor of 5 too high (J. Black 2002, private communication), or K I may not scale linearly with Li I.

#### 4.3. Elemental Abundances

The derivation of the total interstellar abundance requires knowledge of the abundance of Li II and the amount of depletion onto grains. In interstellar space, atoms of Li are predominantly singly ionized in view of the fact that the ionization potential of Li I is relatively low (5.31 eV). The ionization potential of Li II is 75.6 eV. We consider the gas phase abundance here and wait to discuss implications for depletion onto grains (§5.2). An adequate estimate of the Li abundance is obtained through ionization balance and an independent determination of the electron density ( $n_e$ ). The electron density is inferred

directly from the column of  $C^+$ , the most abundant element providing electrons, the gas density ( $n$ ) (Federman et al. 1994; Knauth et al. 2001), and the total proton column density [ $N_{tot}(H) = N(H\ I) + 2N(H_2)$ ] (Savage et al. 1977; Bohlin et al. 1978; Diplas & Savage 1994) along the LOS. Table 6 contains the information on  $N(H\ I)$ ,  $N(H_2)$ ,  $N_{tot}(H)$ , and  $n$ . Since no precise interstellar measurements of  $C^+$  exist for the clouds toward  $o\ Per$ ,  $\chi\ Oph$ , and  $20\ Aql$ , the weighted mean interstellar ratio of  $N(C^+)/N_{tot}(H) = (1.42 \pm 0.13) \times 10^{-4}$  (Sofia, Cardelli, & Guerin 1997) was utilized. Precise measures of  $N(C^+)/N_{tot}(H)$  are used in the analysis toward  $X\ Per$  [ $(1.06 \pm 0.38) \times 10^{-4}$ ; Sofia, Fitzpatrick, & Meyer 1998] and toward  $\zeta\ Oph$  [ $(1.32 \pm 0.32) \times 10^{-4}$ ; Cardelli et al. 1993]. Welty & Hobbs (2001) discussed the effects of large molecules on ionization balance and found that depletion (or elemental abundances) of Li, Na, and K are not altered appreciably.

Through ionization balance we can determine the gas phase lithium abundance (Li/H), without a correction for depletion onto grains, via

$$A_g(\text{Li}) = \text{Log} \left( \left[ \frac{N(\text{Li I})}{N_{tot}(\text{H})} \right] \left[ \frac{G(\text{Li I})}{\alpha(\text{Li II})n_e} \right] \right) + 12. \quad (1)$$

In this equation,  $A_g(\text{Li})$  is the elemental abundance,  $\alpha(\text{Li II})$  is the radiative recombination rate constant (Péquignot & Aldrovandi 1986),  $G(\text{Li I})$  is the photoionization rate from the ground state corrected for attenuation by dust grains. The theoretical determination of  $\alpha(\text{Li II})$  depends on the photoionization cross section from all levels and is known to better than 2.5% (Péquignot & Aldrovandi 1986). The photoionization rates at the cloud surface were determined from the measured ionization cross sections of Hudson & Carter (1965a, 1967a) and the average interstellar radiation field of Draine (1978). A similar expression holds for  $A_g(\text{K})$ , where K I rates were determined from the measured ionization cross sections of Hudson & Carter (1965b, 1967b), Marr & Creek (1968), and Sandner et al. (1981).

The photoionization rates need to be corrected for the effect of attenuation from dust in the interstellar cloud(s). This is accomplished through use of extinction curves for the particular line of sight. If one were to assume that all dust particles are the same throughout the Galaxy, one would get an average Galactic extinction curve (Code et al. 1976).

From the extinction curves (Papaj, Krewlowski, & Wegner 1991), the value of selective extinction,  $A_\lambda$ , for the reddened star, can be derived with the equation,

$$A_{\lambda*} = \frac{E(\lambda - V)}{E(B - V)} E(B - V) + A_{V*}. \quad (2)$$

Eqn. 2 assumes there is no interstellar extinction along the line of sight toward the unred-



dened star. This is generally not the case; therefore we need to include terms for selective extinction for the unreddened star,  $A_{\lambda_o}$  and  $A_{V_o}$ . These values of selective extinction were obtained from the average Galactic extinction curve (Code et al. 1976) scaled to the  $E(B - V)$  of the unreddened star, typically 0.02 magnitudes.

Correcting the photoionization rates for attenuation involves a multiplicative factor of the form  $\exp(-\tau_\lambda)$ , where  $\tau_\lambda = A_\lambda/2$ . The factor of 2 arises because radiation impinges from both sides of the slab representing a cloud. An optical depth ( $\tau_{1200}$ ) was chosen for Li I, since 1200 Å lies in the middle of the range in wavelength that leads to its photoionization. Two optical depths were used for K I:  $\tau_{1200}$  for the overlap region and  $\tau_{2500}$  for wavelengths longer than 2400 Å, which do not contribute to the photoionization of Li I. The total attenuated photoionization rate for potassium comprises the sum for the two intervals. The long wavelength interval contributes about 5% to the total. For most of the observed lines of sight, the extinction curves are similar to the standard extinction curve (Code et al. 1976), the exceptions being X Per and  $\chi$  Oph. These anomalous extinction curves arise because X Per is a member of an x-ray binary system and  $\chi$  Oph is an emission line star. The different extinction laws change the photorates by approximately 20 – 30% compared to the standard extinction curve; larger excursions result for the anomalous extinction curves of X Per ( $\sim$  70%) and  $\chi$  Oph ( $\sim$  40%).

The derived interstellar lithium abundances, shown in Table 7, are quite similar to other recent determinations with the exception of X Per and 20 Aql. The LOS toward X Per exhibits almost an order of magnitude lower Li abundance than other sight lines, while the Li abundance toward 20 Aql is about a factor-of-2 less. Using the above analysis for consistency, previous measures are:  $2.9 \times 10^{-10}$  toward  $\sigma$  Per (Knauth et al. 2000);  $3.3 - 3.6 \times 10^{-10}$  toward  $\zeta$  Per (Meyer et al. 1993; Knauth et al. 2000);  $2.7 \times 10^{-10}$  toward  $\rho$  Oph (Lemoine et al. 1993); and  $3.9 - 4.9 \times 10^{-10}$  toward  $\zeta$  Oph (Meyer et al. 1993; Lemoine et al. 1995). These values are different from those presented in the referenced work because they include our correction for the attenuation of the radiation field and use a different photoionization rate.

#### 4.4. Depletion onto Grains

The determination of the elemental Li abundance requires an uncertain correction for the amount of depletion onto grains. From the gas phase Li/H abundance, the amount of Li depletion onto grains was estimated. The amount of depletion is measured with respect to the Solar System value from meteorites,  $\text{Log}((\text{Li}/\text{H})_*/(\text{Li}/\text{H})_\odot)$ , where  $(\text{Li}/\text{H})_\odot = 20.5 \times 10^{-10}$  (Anders & Grevesse 1989). The K depletion was derived in a similar manner using the

value of  $(\text{K}/\text{H})_{\odot} = 1.26 \times 10^{-7}$  (Anders & Grevesse 1989). One problem with the use of the Solar System values for depletion measures is the assumption that the Solar System value represents undepleted gas in the solar neighborhood. There is evidence (Wielen, Fuchs, & Dettbarn 1996; Wielen & Wilson 1997) that the Sun actually formed closer to the center of the Galaxy, by about 2 kpc. If our Sun formed in a more metal-rich environment, then the comparison with the Solar System values is inappropriate. Furthermore, the Solar System values represent the interstellar gas at the epoch of formation, 4.6 Gyr ago.

The amounts of depletion, given by the depletion indices  $D(\text{Li})$  and  $D(\text{K})$ , are listed in Table 7. The indices for Li and K are similar for most sight lines ( $\sim -0.9$  dex), with the exceptions of those toward X Per and 20 Aql which are discussed in more detail below. Welty & Hobbs (2001) also reported similar amounts of depletion for the two species, but for a larger number of sight lines. Their depletion indices are  $D(\text{K}) \sim D(\text{Li}) \sim -0.6$  dex. The use of a constant index for Li and K just scales the gas phase abundance without revealing any new information; direct comparison to the Solar System may be more appropriate in studying effects of depletion onto grains.

#### 4.5. Elemental K/Li Ratio

Through the comparison of  $N(\text{Li I})$  and  $N(\text{K I})$  – see §4.2, Welty & Hobbs (2001) suggest a constant elemental K/Li abundance ratio. It is straightforward to calculate the elemental K/Li abundance ratio and compare it with the Solar System value on a component-by-component basis for our results. Since the amount of depletion onto grains is similar for the two species (Welty & Hobbs 2001) for most directions, its uncertainty in Eqn. 1 can be minimized by taking the ratio of  $N(\text{K I})$  to  $N(\text{Li I})$ . This ratio, which also eliminates  $n_e$  and  $N_{tot}(\text{H})$ , is represented by

$$\left[ \frac{A_g(\text{K})}{A_g(\text{Li})} \right] = \left[ \frac{N(\text{K I})}{N(\text{Li I})} \right] \left[ \frac{\alpha(\text{Li II})}{\alpha(\text{K II})} \right] \left[ \frac{G(\text{K I})}{G(\text{Li I})} \right], \quad (3)$$

where the observed values were compared to the Solar System value for  $A_g(\text{K})/A_g(\text{Li})$  of 61.6 (Anders & Grevesse 1989). Using the theoretical ratio for  $\alpha(\text{K II})/\alpha(\text{Li II}) = 0.58$  (Péquignot & Aldrovandi 1986), the K/Li ratio then mainly depends on the photoionization rates for K I and Li I.

For the best fit velocity structure (§4.1), the calculated elemental K/Li abundance ratios are consistent with the Solar System value of 61.6 (Anders & Grevesse 1989), considering their mutual uncertainties – see Table 8. On the other hand, both significantly higher

and lower abundance ratios result when other component structures are considered. We, therefore, suggest that the K/Li ratio can be used to discriminate between syntheses based on different velocity structure. For the LOS toward X Per, both Li and K abundances are low by a comparable amount and thus the K/Li ratio is unaffected. This suggests that the amount of depletion onto grains is substantially greater or that  $n_e$  has been underestimated. The one exception is the LOS toward 20 Aql; both components yield elemental K/Li abundance ratios that are about two times larger. As an additional check for this line of sight, our previous high-resolution data on K I  $\lambda 7699$  (Knauth et al. 2001) were reanalyzed with the velocity component structure deduced from our UHR data. This reanalysis yielded similar  $N(\text{K I})$  and elemental K/Li abundance ratios to those obtained from  $\lambda 4044$ . Therefore the disparate K/Li ratios toward 20 Aql appear to be real. The discrepancy could be the result of an increase (decrease) in the photoionization rate of Li (K), of evidence for enhanced depletion of Li compared to K, or of the possibility that Li production (destruction) was lower (higher) along this LOS. The low K/Li ratios toward 20 Aql are discussed further in §6.

## 5. Interstellar Matters

### 5.1. Detecting Lithium

At our resolution, velocity structure separated by  $\sim 1 \text{ km s}^{-1}$  can be resolved (e.g.  $\zeta$  Oph). Most of the additional velocity structure detected in K I  $\lambda 7699$  (Welty & Hobbs 2001) is separated by more than  $1 \text{ km s}^{-1}$  and should be resolved in our data. This situation is reminiscent of the component structure utilized by Lemoine et al. (1995) for the gas toward  $\zeta$  Oph. Because its  $f$ -value is much larger, K I  $\lambda 7699$  reveals components too weak to see in absorption from either K I  $\lambda 4044$  or Li I  $\lambda 6707$ . Although  $\lambda 7699$  is not an ideal template for velocity structure, it plays an important role in the search for Li I by revealing sight lines where Li I may be detectable.

In addition to absorption from K I, another useful means for determining lines of sight having detectable amounts of Li I is the amount of molecular material present – i.e., CH,  $\text{C}_2$ , or CN. Atoms with low IPs and molecules exist only in the relatively denser regions of diffuse gas. The molecular column densities for the lines of sight studied here are presented in Table 9. For sight lines where Li I is found, significant amounts of molecular absorption are also observed (e.g.,  $N(\text{CH}) \approx N(\text{C}_2) \approx 10^{13} \text{ cm}^{-2}$ ;  $N(\text{CN}) \geq 10^{12} \text{ cm}^{-2}$ ). Since 40 Per and  $\lambda$  Ori are in regions of active star formation and have relatively strong K I  $\lambda 7699$  absorption, they were considered potential targets. However, no Li I was detected; of all stars observed in our survey, 40 Per has the lowest values for  $N(\text{C}_2)$  and  $N(\text{CN})$  and  $\lambda$  Ori has the lowest

value of  $N(\text{H}_2)$  – see Table 6. Therefore the amount of molecular material present along a given LOS seems a superior indicator for detectable amounts of Li I.

## 5.2. Thermal vs. Turbulent Broadening

Atoms of K I and Li I seem to reside in the same portion of interstellar clouds. Through measurements of the  $b$ -value for lines of each species, the kinetic temperature,  $T_k$ , and the turbulent velocity,  $v_{turb}$ , can be extracted,

$$b^2 = \frac{2kT_k}{m} + 2v_{turb}^2. \quad (4)$$

The parameters  $k$  and  $m$  are the Boltzmann constant and the mass of the atom observed. The measured  $b$ -values for each species for individual velocity components along a given LOS are listed in Table 5. The  $b$ -values for Li are generally larger than those for K, with the exception of the LOS toward X Per and  $\zeta$  Oph. If  $v_{turb}$  is assumed to be negligible, an upper limit can be placed on the kinetic temperature. The upper limit on  $T_k$  for all eight lines studied here ranges from 100 K to 2,700 K, values not unexpected for diffuse interstellar clouds. The kinetic temperature and turbulent velocity can be determined simultaneously, since there are two independent measures of the  $b$ -value. The calculated values of  $T_k$  and  $v_{turb}$  for each velocity component are given in Table 10. The uncertainties are based on an assumed 30% error in the  $b$ -values for both species.

In order to arrive at a solution for  $v_{turb}$  for the second component toward  $o$  Per, both components toward X Per, and the single component toward  $\chi$  Oph, extreme values of the  $b$ -value ( $\pm 1\sigma$ ) were utilized. No error bars are quoted for  $T_k$  or  $v_{turb}$  for these components. The derived temperatures for the two components toward  $o$  Per are  $98 \pm 42$  K and 900 K and those toward X Per are 520 K and 788 K. For the single component toward  $\chi$  Oph, a temperature of 220 K is inferred. The two components toward  $\zeta$  Oph yield temperatures of  $61 \pm 27$  K and  $63 \pm 27$  K and toward 20 Aql the temperatures are  $287 \pm 124$  K and  $770 \pm 330$  K. The current measurements agree with previous determinations of  $T_k$ , to within the assumed uncertainties. From  $\text{H}_2$  excitation, Savage et al. (1977) deduced temperatures of 48 K toward  $o$  Per, 46 K toward  $\chi$  Oph, and 54 K toward  $\zeta$  Oph. From  $\text{C}_2$  excitation and a simple chemical model for CH,  $\text{C}_2$ , and CN (Federman et al. 1994), temperatures of 40 K toward  $o$  Per, 20 K toward X Per, 60 K toward  $\chi$  and  $\zeta$  Oph (Federman et al. 1994), and 50 – 60 K toward 20 Aql (Federman, Strom, & Good 1991; Hanson, Snow, & Black 1992; Knauth et al. 2001) are derived. From an analysis of  $\text{C}_2$  excitation, Wannier et al. (1999) derived a temperature of  $40 \pm 20$  for the LOS toward  $o$  Per and Lambert, Sheffer,

& Federman (1995) derived a temperature of 20 – 80 K for the interstellar clouds toward  $\zeta$  Oph. Howarth et al. (2002) found  $T_k$  of  $500 \pm 130$  K and  $830 \pm 125$  K toward  $\zeta$  Oph. Their higher temperatures are primarily due to their larger derived  $b$ -values for Li I.

The turbulent velocities were determined for each velocity component as well as  $T_k$ . Our calculated values of  $v_{turb}$  for both interstellar clouds toward  $\zeta$  Oph are  $0.38 \pm 0.20$  and  $0.30 \pm 0.16$  km s<sup>-1</sup>. These values agree well with previous determinations,  $0.39_{-0.10}^{+0.04}$  and  $0.33_{-0.16}^{+0.37}$  km s<sup>-1</sup>, based on UHR spectra of CH and CN (Crawford et al. 1994). This agreement with an independent measure places additional confidence in  $v_{turb}$  obtained for the other sight lines. With the exception of the second component toward  $o$  Per and the LOS toward X Per, the turbulent velocities are substantially less than 1 km s<sup>-1</sup>. For further comparison,  $v_{turb}$  was calculated assuming  $T_k = 100$  K, a typical value for diffuse clouds. A comparison between  $v_{turb}$  and the sound speed shows that the turbulence is subsonic for all sight lines. The inclusion of molecular gas decreases the sound speed slightly and in some instances may lead to sonic turbulence.

## 6. Interstellar <sup>7</sup>Li/<sup>6</sup>Li Ratios - the rule

With the exception of one cloud along the line of sight to  $o$  Per and possibly the line of sight toward  $\zeta$  Oph, our lower limits and the few other published <sup>7</sup>Li/<sup>6</sup>Li ratios are consistent with an expectation that interstellar Li should be similar to the Solar System ratio of <sup>7</sup>Li/<sup>6</sup>Li = 12.3 (Anders & Grevesse 1989). This expectation is based on observational evidence that young stars and interstellar gas have a composition quite similar to that of the Sun for elements whose synthesis is traceable to the same sites likely to control the <sup>7</sup>Li and <sup>6</sup>Li input into the interstellar medium. Beryllium and <sup>6</sup>Li are both products of spallation between Galactic cosmic rays and interstellar nuclei. The stellar abundances of Be in local stars younger than the Sun is very similar to the Solar System abundance (Boesgaard et al. 2001). Oxygen, a product of SN II which may also make <sup>7</sup>Li by the  $\nu$ -process, has very similar abundances in the Sun, young stars, and the interstellar medium (Allende Prieto, Lambert, Asplund 2001). Carbon, partly a product of AGB stars which may also synthesize <sup>7</sup>Li, also shares a similar abundance with Sun, young stars, and the local interstellar medium (Allende Prieto, Lambert, & Asplund 2002). Another line of evidence to support the expectation of similar isotopic ratios among the clouds and the Solar System is that stars of solar metallicity show very similar abundance ratios for elements created by different nucleosynthetic processes despite differences in age and birthplace (Edvardsson et al. 1993; Reddy et al. 2002).

The expectation applies to the total Li abundance too. Since about 90% of interstellar

Li is depleted onto or into grains, the K/Li ratio is considered. Identification of this ratio with the elemental ratio assumes depletion of Li and K, both alkali atoms, is similar. Table 8 shows that seven of the nine clouds have a K/Li ratio close to the Solar System ratio of 61.6: the mean of the 7 clouds is 62.4 and individual measurements are each consistent with the Solar System value to within their mutual uncertainties. Our previous observations toward  $\zeta$  Per (Knauth et al. 2000) yield a K/Li ratio of  $52.6 \pm 3.4$ . The average of eight additional K/Li ratios from Welty & Hobbs (2001) is 59, assuming that a standard extinction curve applies for all sight lines. With the exception of 20 Aql, all K/Li ratios are consistent with the Solar System value.

The interstellar clouds, toward stars studied here, have depletion indices ranging from 0.7 to 1.5 dex (assuming solar Li and K abundances). The sight line with the largest depletion, X Per, is the most reddened direction. The other two clouds, the pair toward 20 Aql, have  $K/Li \simeq 116$ , a value about twice the Solar System ratio. Several speculations may be offered for the anomalous ratios toward 20 Aql: (i) the spectrum of the ionizing radiation is different from that assumed; (ii) Li (relative to K) is more depleted onto grains; or (iii) the gas may have been mixed with ejecta –now cold – from the supernova thought to be responsible for Radio Loop I (Hayakawa et al. 1979; Sembach, Savage, & Tripp 1997). Factors of two spreads in abundance ratios are not uncommon; Welty & Hobbs (2001) discuss a collection of ‘discrepant’ clouds toward the Sco-Oph region.

## 7. Interstellar ${}^7\text{Li}/{}^6\text{Li}$ Ratios - the exception?

One of the clouds toward  $o$  Per has an exceptional  ${}^7\text{Li}/{}^6\text{Li}$  ratio of  $2.1 \pm 1.1$ . This is clearly shown by spectra taken with two different spectrographs. Our previous lower resolution data shown in Figure 6 clearly shows that a Solar System ratio cannot apply to either interstellar cloud toward  $o$  Per. From a visual examination of the data, both components are in almost a one-to-one correspondence and not in the two-to-one relation expected from atomic physics. The apparent disagreement in the  ${}^7\text{Li}/{}^6\text{Li}$  isotope ratio for the second component, between our current and previous measurements, could be due to an undetected CCD defect and/or the sole use of the observational errors in determining the uncertainties of the profile synthesis.

In interpreting the low isotope ratio, possible scenarios include: (i) an interloper providing  ${}^7\text{Li}$  at the wavelength of the  ${}^6\text{Li}$  line; (ii) fractionation of the Li isotopes leading to an incorrect isotopic ratio for Li atoms in the gas; or (iii) a local change in the isotopic ratio arising from synthesis of Li isotopes.

Thinner clouds than detectable from our 4044 Å spectra are revealed by spectra of the 7699 Å K I and Na D lines. If the absorption attributed to  ${}^6\text{Li}$  is in fact  ${}^7\text{Li}$  with a column density of about  $2 \times 10^8 \text{ cm}^{-2}$ , a typical diffuse cloud should have a K I column density of about  $4 \times 10^{10} \text{ cm}^{-2}$ , and a detectable line at 7699 Å. Its 4044 Å counterpart would have an  $W_\lambda < 0.1 \text{ mÅ}$  and be indistinguishable from the noise in the spectrum shown in Figure 1 (top panel). The fifth cloud shown by Welty & Hobbs has a column density of  $3.9 \times 10^{10} \text{ cm}^{-2}$ , but it is displaced to the red from the parent  ${}^7\text{Li}$  line by about  $4.7 \text{ km s}^{-1}$  not the by  $7.1 \text{ km s}^{-1}$  that is the isotopic shift. However, inclusion of this red component into the  ${}^7\text{Li}$  profile synthesis does not resolve the low isotope ratio.

Even thinner clouds are detectable in the Na D lines. Welty & Hobbs (2001) found two additional clouds to the red of the two in Figure 1. The velocities are  $+10.6$  and  $+14.0 \text{ km s}^{-1}$  with Na I column densities of  $4.9 \times 10^{10} \text{ cm}^{-2}$  and  $2.5 \times 10^{10} \text{ cm}^{-2}$ , respectively (D. Welty 2001, private communication). The  $10.6 \text{ km s}^{-1}$  cloud’s stronger  ${}^7\text{Li}$  line needs to be at  $+11.1 \text{ km s}^{-1}$  to be mistaken for  ${}^6\text{Li}$  in the weaker of our two clouds. However, if the  $+10.6 \text{ km s}^{-1}$  cloud has a normal Na I/Li I ratio, the expected Li I column density is almost 2 orders of magnitude less than that required to account for the  ${}^6\text{Li}$ . Incorporation of these two additional velocity components into the profile synthesis yields a reasonable fit to the data and obtains  ${}^7\text{Li}/{}^6\text{Li}$  ratios that are all consistent with the Solar System value. Unfortunately, this scenario solves the  ${}^6\text{Li}$ -problem by replacing it with another one - how to account for the very discrepant Na I/Li I and K I/Li I ratios yet normal Na I/K I ratios.

Fractionation of the Li isotopes is an improbable scenario on several accounts. Even if no  ${}^6\text{Li}$  is removed from the gas, the total Li abundance must drop by a factor of about 4, which would place the cloud off the tight relation in Figure 7, unless K is also removed. In addition, we have been unable to identify a plausible fractionation process: the predicted abundances of Li-containing molecules (Kirby & Dalgarno 1978) are orders of magnitude too low; ionization and recombination are isotopically insensitive; gas-dust grain processes would seem not to be dependent on the mass difference between the isotopes.<sup>5</sup> Therefore, it is unlikely that  ${}^7\text{Li}$  is hiding in another neutral species.

A close correspondence between the exceptional  ${}^7\text{Li}/{}^6\text{Li}$  ratio and that resulting from either spallation of C, N, and O or  $\alpha + \alpha$  fusion reactions encourages speculation that the ratio reflects freshly synthesized lithium. The speculation faces at least two hurdles. (i) Why is the K/Li ratio of the exceptional cloud that of a normal cloud where local synthesis of Li is not invoked? (ii) What is the energy source for the particles causing the spallation and

---

<sup>5</sup>If the grains originate in circumstellar atmospheres of red giants, they will be Li-poor in the main. Then, evaporation of grains will produce a local dilution of the Li/K ratio but no change in the  ${}^7\text{Li}/{}^6\text{Li}$  ratio.

fusion reactions?

Omicron Per is a member of the Per OB2 Association and the line of sight lies close to IC 348, an active region of star formation. The association, as would be expected, has experienced supernovae. X Per is a O9.5Ve star orbiting a neutron star (Delgado-Martí et al. 2001) and  $\xi$  Per is a runaway star (Hoogerwerf, de Bruijne, & de Zeeuw 2001). Consideration of the chemistry of OH and HD led Federman et al. (1996) to the conclusion that the interstellar clouds toward *o* Per are permeated by an order of magnitude higher cosmic ray flux than clouds seen toward other stars in Per OB2. The enhanced cosmic rays could indicate that we are looking at a young superbubble where dilution has not yet occurred.

The energetics required to synthesize the observed amount of Li toward *o* Per may reveal vital information for understanding Li production in interstellar space. Assuming spherical geometry and using  $N_{tot}(\text{H})$  and  $n$  from Table 6, we find that 2.2 solar masses of hydrogen are present in the interstellar clouds toward *o* Per. Assuming that the clouds have the Solar System Li abundance ( $\text{Li}/\text{H}_{\odot} = 20.5 \times 10^{-10}$ ) implies that there are  $5.4 \times 10^{48}$  atoms of Li in the clouds. Approximately 3 ergs of energy are needed to create a single atom of Li (Ramaty et al. 1996). Therefore, to reproduce the entire Li content in the clouds toward *o* Per requires approximately 1% of the energy output of a typical supernova explosion. Models of superbubbles (Parizot & Drury 1999) show that the Li production per SN II is approximately  $10^{50}$  atoms. The superbubble picture may apply for the interstellar clouds toward *o* Per. We note that Li is not produced solely through supernova explosions.

Studies show large variable x-ray fluxes in IC 348 (Preibisch, Zinnecker, & Herbig 1996) that are attributed to flares produced in T Tauri stars (Preibisch, Neuhäuser, & Alcalá 1995). The total x-ray luminosity is on the order of  $10^{32}$  erg s<sup>-1</sup> (Preibisch et al. 1996). If all 116 x-ray sources (Preibisch et al. 1996) contribute, with flares lasting on the order of 10 hours, the total energy produced is  $4 \times 10^{38}$  ergs, enough for about  $10^{38}$  atoms of <sup>6</sup>Li. This calculation assumes that all flare energy goes into the creation of <sup>6</sup>Li. The amount of <sup>6</sup>Li that can be created by stellar flares is about 10 orders of magnitude less than that needed to reproduce the entire <sup>6</sup>Li content of the interstellar clouds toward *o* Per. X-ray flares with energies on the order of  $10^{38}$  ergs have been reported (Preibisch et al. 1995). Even in these extreme cases, <sup>6</sup>Li production is negligible; therefore x-ray flares cannot produce the observed <sup>6</sup>Li abundance. A further complication is that this process is not isotope selective since <sup>7</sup>Li is formed as well.



## 8. Constraints on Stellar Source of ${}^7\text{Li}$

The isotope ratios given in Table 5 provide important constraints on stellar production pathways for  ${}^7\text{Li}$  (Reeves 1993; Steigman 1993). The abundance of  ${}^7\text{Li}$  arises from several processes: BBN, GCR spallation reactions, and stellar production mechanisms. During the early Universe, BBN supplied about 10% of the present  ${}^7\text{Li}$  and a negligible amount of  ${}^6\text{Li}$ . GCR spallation reactions contribute another 10 – 25% of  ${}^7\text{Li}$  and account for the present abundance of  ${}^6\text{Li}$ . Although the nature of the stellar source of  ${}^7\text{Li}$  is still unclear, it plays the most important role in Li production today.

There has been much debate over which stellar source dominates  ${}^7\text{Li}$  production throughout the lifetime of the Galaxy. As noted in the Introduction, the various stellar sources of  ${}^7\text{Li}$  are thought to be primarily AGB and RGB stars, SN II, and possibly novae. Although AGB have been observed with the largest Li abundances, recent models of Galactic chemical evolution have all but eliminated AGB stars as contributors to the Galactic  ${}^7\text{Li}$  abundance (Charbonnel & Balachandran 2000; Romano et al. 2001). As for the  $\nu$ -process in SN II, the yields of  ${}^{11}\text{B}$  and therefore  ${}^7\text{Li}$  have been called into question. Alibes, Labay, and Canal (2001) suggest a reduction by a factor of 2 in the yields of Woosley and Weaver (1995). A problem with the source being novae is the lack of observational evidence (Andrea, Drechsel, & Starrfield 1994; Matteucci, D’Antona, & Timmes 1995). Since stars have the greatest effect on the  ${}^7\text{Li}$  production today, constraints are needed to isolate the stellar source(s).

Knowledge of the  ${}^6\text{Li}$  abundance yields the amount of  ${}^7\text{Li}$  produced via GCR spallation because the isotope ratio predicted from these reactions ( $R_{76,GCR}$ ) is known with sufficient accuracy (Ramaty et al. 1997; Lemoine et al. 1998). The isotope ratio used here is  $R_{76,GCR} = 1.6$ , which is midway between the values presented by Ramaty et al. (1997). If the  ${}^7\text{Li}$  abundance in halo stars represents the primordial abundance (Ryan et al. 2000, 2001; Suzuki et al. 2000), then the BBN contribution is fairly well known. Additional support for Li in halo stars representing the primordial abundance comes from recent determinations of the  ${}^7\text{Li}/{}^6\text{Li}$  ratio (Smith, Lambert, & Nissen 1993; Hobbs & Thorburn 1994, 1997; Hobbs, Thorburn, & Rebull 1999). These measurements show that there has been little or no nuclear depletion of  ${}^7\text{Li}$  during the lifetimes ( $\sim 12$  Gyr) of these stars. Observations of  ${}^6\text{Li}$  in halo stars also yield a measure of the contamination of the primordial  ${}^7\text{Li}$  through GCR spallation reactions. Recent theoretical determinations of the primordial Li abundance find  $A(\text{Li})_p = 2.09$  (Suzuki et al. 2000), or  $(\text{Li}/\text{H})_p = 1.23 \times 10^{-10}$ . The following equation allows the removal of the “known” sources of  ${}^7\text{Li}$  from the present interstellar abundance.  ${}^7\text{Li}_{stars}$  represents the combined contribution from all stellar sources (AGB, RGB, SN II, & novae),

$${}^7\text{Li}_{stars} = {}^7\text{Li}_{ISM} - {}^6\text{Li}_{ISM} * R_{76,GCR} - {}^7\text{Li}_p. \quad (5)$$

Also included in  ${}^7\text{Li}_{stars}$  is the amount of destruction by stellar astration.

The Li abundances corrected for our estimates of depletion onto grains and the amount of  ${}^7\text{Li}$  produced through GCR spallation reactions are presented in Table 11. The amount of  ${}^7\text{Li}$  produced by all stellar sources (using our depletion index) is similar, approximately  ${}^7\text{Li}/\text{H} \sim 1 \times 10^{-9}$  for all lines of sight. A larger spread arises ( $-5.7 \times 10^{-12} - 1.5 \times 10^{-9}$ ) when utilizing a constant depletion index (Welty & Hobbs 2001), suggesting that use of a constant depletion index may not be appropriate. Since  ${}^7\text{Li}$  production through the various stellar sources in our sample of sight lines is essentially constant, we infer that one or two stellar processes dominate Li production in the solar neighborhood. This may not be unreasonable given the relatively small volume of the Galaxy studied.

Comparison with other elements and isotopic ratios are needed as well. A recent study (Sofia, Meyer, & Cardelli 1999) showed that several lines of sight toward Orion exhibit large interstellar Sn (an s-process element) abundances. Sofia et al. (1999) attribute this Sn overabundance to AGB stars. Since AGB stars and SN II explosions also generate Li, simultaneous observations of Li, s-process, and r-process elements are needed to constrain the amounts of Li production by these two stellar sources. Comparisons of r-process and s-process elements in stars are important for determining which stellar processes contribute to the production of these elements. Knowledge of the  ${}^{12}\text{C}/{}^{13}\text{C}$  and oxygen isotope ratios is useful in constraining the production of Li in RGB stars. For instance, there could be a low  ${}^{12}\text{C}/{}^{13}\text{C}$  ratio in stars with high Li abundance (Sackmann & Boothroyd 1999), but Charbonnel and Balachandran (2000) predict that the high  ${}^7\text{Li}$  abundances will be followed by the rapid destruction of both  ${}^7\text{Li}$  and  ${}^{12}\text{C}$ . Therefore, stellar and interstellar studies are required to disentangle the contributions from the different stellar sources.

## 9. Conclusions

The interstellar Li abundance and the  ${}^7\text{Li}/{}^6\text{Li}$  isotope ratio were measured toward several bright stars in the solar neighborhood. These observations form the highest resolution ( $R \sim 360,000$ ) survey of interstellar Li to date. From these data it appears that the Li abundance has not significantly changed since the formation of the Solar System and that the Solar System value of  $\sim 12$  for the  ${}^7\text{Li}/{}^6\text{Li}$  ratio represents most of the gas in the solar neighborhood. One exception is the LOS toward *o* Per. This sight line exhibits a low  ${}^7\text{Li}/{}^6\text{Li}$  ratio of about 2, the value expected from models of GCR spallation reactions, which is consistent with our previous determination (Knauth et al. 2000) from lower resolution observations.

If a value of about 12 was the starting condition for the gas toward *o* Per, the decrease in the ratio to its present value requires an increase in the Li abundance by an order of magnitude. However, an enhancement in the total Li abundance is not seen. The elemental K/Li ratio for this gas is not unusual either, although K and Li are produced via different nucleosynthetic pathways. The most likely scenario for the ISM toward *o* Per is that the initial Li was enhanced through GCR spallation reactions occurring as a result of recent supernovae grouped in a superbubble. The cloud containing a low isotope ratio contains about 20% of the total Li content of the clouds. Therefore, determination of a total Li abundance may mask the true Li abundance for each interstellar cloud. Although the supernova scenario explains many of the observations, this hypothesis does not address the similarity of the K/Li ratio with results for other sight lines. Fractionation cannot account for the low  ${}^7\text{Li}/{}^6\text{Li}$  ratio because the abundance of LiH is too small. There is also evidence for enhanced x-ray activity in the cluster IC 348 caused by stellar flares in T Tauri stars (Preibisch et al. 1996). While  ${}^6\text{Li}$  can be produced during stellar flares (e.g., Deliyannis & Malaney 1995; Ramaty et al. 2000b), the enhanced flaring activity in OB associations was found to play a negligible role. More typical  ${}^7\text{Li}/{}^6\text{Li}$  ratios can be obtained through the inclusion of extra velocity components that are detected in Na I absorption at 5895 Å but not seen in K I absorption at 7699 Å, although this comes at the expense of highly disparate Na I/Li I and K I/Li I ratios. Therefore, the exceptional isotopic ratio toward *o* Per remains a puzzle. Further observations of other stars in or near IC 348 are needed to probe the extent of the region containing a low  ${}^7\text{Li}/{}^6\text{Li}$  ratio.

Observations were made of X Per, a nearby x-ray binary. It is believed that X Per and other x-ray binary systems are formed after a supernova explosion (e.g., Delgado-Martí et al. 2001). The direction toward X Per shows almost an order of magnitude smaller Li and K abundances than toward other sight lines. These smaller abundances suggest enhanced depletion along the LOS. Unfortunately, the SNR of the X Per spectrum was too low to allow a useful probe of the region containing the low isotope ratio.

The stars in Sco OB2 were studied since they closely matched the situation present toward *o* Per. These stars are in an OB association where star formation is occurring in the  $\rho$  Oph molecular cloud. There is evidence of a past supernova because  $\zeta$  Oph is a runaway star (Hoogerwerf et al. 2001). Why is there no evidence for enhanced  ${}^6\text{Li}$  production in the presence of active star formation ( $\rho$  Oph molecular cloud) and past SN II explosions? Is the LOS toward *o* Per really that rare? More observations are necessary to determine if we are experiencing a selection effect; to date, only three sight lines in each OB association have been studied with sufficient precision.

An additional result of our study involves the LOS toward 20 Aql, which resides far

from active star-forming regions. The  ${}^7\text{Li}/{}^6\text{Li}$  ratio is similar to the Solar System value, but the K/Li ratio is almost double the expected value. The K/H abundance is similar to the abundance found for other sight lines, indicating that there is less Li. The LOS toward 20 Aql lies on the edge of Radio Loop I (Hayakawa et al. 1979; Sembach, Savage, Tripp 1997), a superbubble. However, the timescale needed to destroy Li through proton burning is significantly longer than the age of bubble. Another explanation is required to account for the low Li/H abundance. The low Li abundance toward 20 Aql could be evidence for Li dilution in an old superbubble (Parizot & Drury 1999; Knauth et al. 2000). Observations of Li I and K I toward other stars in the vicinity of 20 Aql are necessary to gain further insight.

We place additional interstellar constraints on the  ${}^7\text{Li}$  produced by a stellar source. Our results indicate that there is essentially a constant production of  ${}^7\text{Li}$  in stars in the solar neighborhood, suggesting one or two processes dominate. Observations of interstellar and stellar  ${}^7\text{Li}$ , s-process, and r-process elements can be of great value in constraining the Li production by the various stellar sources.

For future studies of interstellar Li, knowledge of the K I abundance in conjunction with the molecular content can be used to find sight lines that contain observable amounts of Li. For instance, the results of this survey suggest other targets in Sco OB2. These stars, which are fainter than X Per, can be observed at lower resolving power ( $R \sim 180,000$ ) because their interstellar spectra reveal simple velocity structure. Preliminary results for these stars indicate that the  ${}^7\text{Li}/{}^6\text{Li}$  ratios are similar to the Solar System value. Thus, lines of sight with low  ${}^7\text{Li}/{}^6\text{Li}$  ratios appear to be rare. Observations of stars in the vicinity of IC 348 (in Per OB2) are planned to help clarify the picture for gas toward  $\sigma$  Per. In addition, data from the *Hubble Space Telescope* on the interstellar  ${}^{11}\text{B}/{}^{10}\text{B}$  ratio toward stars in Per OB2 are being analyzed. The interstellar abundance of  ${}^9\text{Be}$  and the  ${}^{11}\text{B}/{}^{10}\text{B}$  ratio (Hebrard et al. 1997; Lambert et al. 1998) are crucial to our understanding of Li evolution. Knowledge of  ${}^9\text{Be}$  and  ${}^{10}\text{B}$  further constrain the amount of GCR spallation occurring along the line of sight, since GCR spallation is the only production route for these light elements. Observations of interstellar  ${}^9\text{Be}$  are not yet feasible because its gas phase abundance is extremely low ( ${}^9\text{Be}/\text{H} \leq 7 \times 10^{-13}$ ; Hebrard et al. 1997). The amount of  ${}^{11}\text{B}$  also yields constraints on SN II explosions because about 50% of  ${}^{11}\text{B}$  is thought to arise from neutrino-induced spallation reactions (Woosley et al. 1990; Woosley & Weaver 1995). Only through a more complete study of the abundances for a variety of atomic species will the light element puzzle be resolved.

The McDonald Observatory data presented here formed the basis for David Knauth’s Ph.D. dissertation. It is a pleasure to thank the excellent staff at McDonald Observatory,

especially David Doss, for assistance with the instrumental setup. We also thank János Zsargó for the use of his code. This research made use of the Simbad database, operated at CDS, Strasbourg, France. This research was supported in part by NASA LTSA grant NAG5-4957.

## REFERENCES

- Allende Prieto, C., Lambert, D. L., & Asplund, M. 2001, *ApJ*, 556, L63
- Allende Prieto, C., Lambert, D. L., & Asplund, M. 2002, *ApJ*, 573, L137
- Alibes, A., Labay, J., & Canal, R. 2001, *A&A*, 370, 1103
- Anders, E., & Grevesse, N. 1989, *Geochim. Cosmochim. Acta*, 53, 197
- Andrea, J., Drechsel, H., & Starrfield, S. 1994, *A&A*, 291, 869
- Bevington, P. R., & Robinson, D. K. 1992, *Data Reduction and Error Analysis for the Physical Sciences*, (Boston, WCB McGraw-Hill), 156
- Boesgaard, A. M., Deliyannis, C. P., King, J. R., & Stephens, A. 2001, *ApJ*, 553, 754
- Bohlin, R. C., Savage, B. D., & Drake, J. F. 1978, *ApJ*, 224, 132
- Boothroyd, A. I., Sackmann, I.-J., & Wasserburg, G. J. 1994, *ApJ*, 430, L77
- Boothroyd, A. I., Sackmann, I.-J., & Wasserburg, G. J. 1995, *ApJ*, 442, L21
- Cameron, A. G. W., & Fowler, W. A. 1971, *ApJ*, 164, 111
- Cardelli, J. A., & Ebbets, D. C. 1994, in *Calibrating Hubble Space Telescope, HST Calibration Workshop*, ed. J.C. Blades & S.J. Osmer (Baltimore:STScI), 322
- Cardelli, J. A., Mathis, J. S., Ebbets, D. C., & Savage, B. D. 1993, *ApJ*, 402, L17
- Cassé, M., Lehoucq, R., & Vangioni-Flam, E. 1995, *Nature*, 373, 318
- Charbonnel, C., & Balachandran, S. C. 2000, *A&A*, 359, 563
- Code, A.D., Bless, R.C., Davis, J., & Brown, H. R. 1976, *ApJ*, 203, 417
- Crawford I. A., Barlow, M. J., Diego, F., & Spyromilio, J. 1994, *MNRAS*, 266, 903
- Crawford I. A., & Barlow, M. J. 1996, *MNRAS*, 280, 863

- Delgado-Martí, H., Levine, A. M., Pfahl, E., & Rappaport, S. A. 2001, *ApJ*, 546, 455
- Deliyannis, C. P., & Malaney, R. A. 1995, *ApJ*, 453, 810
- Diplas, A., & Savage, B. D. 1994, *ApJS*, 93, 211
- Draine, B. T. 1978, *ApJS*, 36, 595
- Edvardsson, B., Andersen, J., Gustafsson, B., Lambert, D. L., Nissen, P. E., & Tomkin, J. 1993, *A&A*, 275, 101
- Federman, S. R., Strom, C. J., & Good, J. C. 1991, *AJ*, 102, 1393
- Federman, S. R., Strom, C. J., Lambert, D. L., Cardelli, J. A., Smith, V. V., & Joseph, C. L. 1994, *ApJ*, 424, 772
- Federman, S. R., Weber, J., & Lambert, D. L. 1996, *ApJ*, 463, 181
- Ferlet, R., & Dennefeld, M. 1984, *A&A*, 138, 303
- Fields, B. D., Olive, K. A., Cassé, M., & Vangioni-Flam, E. 2001, *A&A*, 370, 634
- Hanson, M. M., Snow, T. P., & Black, J. H. 1992, *ApJ*, 392, 571
- Hayakawa, S., Kato, T., Nagase, F., Yamashita, K., & Tanaka, Y. 1979, *PASJ*, 31, 71
- Hebrard, G., Lemoine, M., Ferlet, R., & Vidal-Madjar, A. 1997, *A&A*, 324, 1145
- Higdon, J. C., Lingenfelter, R. E., & Ramaty, R. 1998, *ApJ*, 509, L33
- Hobbs, L. M. 1974a, *ApJ*, 188, L67
- Hobbs, L. M. 1974b, *ApJ*, 191, 381
- Hobbs, L. M. 1984, *ApJ*, 286, 252
- Hobbs, L. M., & Thorburn, J. A. 1994, *ApJ*, 428, L25
- Hobbs, L. M., & Thorburn, J. A. 1997, *ApJ*, 491, 772
- Hobbs, L. M., Thorburn, J. A., & Rebull, L. M. 1999, *ApJ*, 523, 797
- Hoogerwerf, R., de Bruijne, J. H. J., & de Zeeuw, P. T. 2001, *A&A*, 365, 49
- Howarth, I. D., Price, R. J., Crawford, I. A., & Hawkins, I. 2002, *MNRAS*, 335, 267
- Hudson, R. D., & Carter, V. L. 1965a, *Phys. Rev.*, 137, A1648

- Hudson, R. D., & Carter, V. L. 1965b, *Phys. Rev.*, 139, A1426
- Hudson, R. D., & Carter, V. L. 1967a, *J. Opt. Soc. Am.*, 57, 651
- Hudson, R. D., & Carter, V. L. 1967b, *J. Opt. Soc. Am.*, 57, 1471
- Kirby, K., & Dalgarno, A. 1978, *ApJ*, 224, 444
- Knauth, D. C., Federman, S. R., Lambert, D. L., & Crane, P. 2000, *Nature*, 405, 656
- Knauth, D. C., Federman, S. R., Pan, K., Yan, M., & Lambert, D. L. 2001, *ApJS*, 135, 201
- Lambert, D. L., Sheffer, Y., & Crane, P. 1990, *ApJ*, 359, L19
- Lambert, D. L., Sheffer, Y., & Federman, S. R. 1995, *ApJ*, 438, 740
- Lambert, D. L., Sheffer, Y., Federman, S. R., Sofia, U. J., & Knauth, D. C. 1998, *ApJ*, 494, 614
- Lemoine, M. 1995, in *The Light Element Abundances*, ed. P. Crane (Garching: European Southern Observatory), p. 350
- Lemoine, M., Ferlet, R., Vidal-Madjar, A., Emerich, C., & Bertin, P. 1993, *A&A*, 298, 879
- Lemoine, M., Ferlet, R., & Vidal-Madjar, A. 1995, *A&A*, 298, 879
- Lemoine, M., Vangioni-Flam, E., & Cassé, M. 1998, *ApJ*, 499, 735
- Lingenfelter, R. E., Ramaty, R., & Kozlovsky, B. 1998, *ApJ*, 500, L153
- Lupton, R. 1993, *Statistics in Theory and Practice*, (Princeton, Princeton University Press), 100
- Marr, G. V., & Creek, D. M. 1968, *Proc. R. Soc. London*, A304, 233
- Mason, K. O., White, R. E., Sanford, P. W., Hawkins, F. J., Drake, J. F., & York, D. G. 1976, *MNRAS*, 176, 193
- Matteucci, F., D'Antona, F., & Timmes, F. X. 1995, *A&A*, 303, 460
- Meneguzzi, M., Audouze, J., & Reeves, H. 1971, *A&A*, 15, 337 (MAR)
- Meyer, D. M., Hawkins, I., & Wright, E. L. 1993, *ApJ*, 409, L61
- Morton, D. C. 1991, *ApJS*, 77, 119

- Papaj, J., Krelowski, J., & Wegner, W. 1991, MNRAS, 252, 403
- Parizot, E., & Drury, L. 1999, A&A, 349, 673
- Pequignot, D., & Aldrovandi, S. M. V. 1986, A&A, 161, 169
- Perryman et al. 1997, A&A, 323, L49
- Plez, B., Smith, V. V., & Lambert, D. L. 1993, ApJ, 418, 812
- Preibisch, T., Neuhaeuser, R., & Alcalá, J. M. 1995, A&A, 304, L13
- Preibisch, T., Zinnecker, H., & Herbig, G. H. 1996, A&A, 310, 456
- Ramaty, R., Kozlovsky, B., & Lingenfelter, R. E., 1996, ApJ, 456, 525
- Ramaty, R., Kozlovsky, B., Lingenfelter, R. E., & Reeves, H. 1997, ApJ, 488, 730
- Ramaty, R., & Lingenfelter, R. E. 1999, Ap&SS, 265, 71
- Ramaty, R., Scully, S. T., Lingenfelter, R. E., & Kozlovsky, B. 2000a, ApJ, 534, 747
- Ramaty, R., Tatischeff, V., Thibaud, J. P., Kozlovsky, B., & Mandzhavidze, N. 2000b, ApJ, 534, 207
- Reddy, B. E., Tomkin, J., Lambert, D. L., & Allende Prieto, C. 2002, MNRAS, submitted
- Reeves, H. 1974, ARA&A, 12, 437
- Reeves, H. 1993, A&A, 269, 166
- Reeves, H., Audouze, J., Fowler, W. A., & Schramm, D. 1973, ApJ, 179, 909
- Reeves, H., Fowler, W. A., & Hoyle, F. 1970, Nature, 226, 727
- Romano, D., Matteucci, F., Ventura, P., & D'Antona, F. 2001, A&A, 374, 646
- Ryan, S. G., Beers, T. C., Olive, K. A., Fields, B. D., & Norris, J. E. 2000, ApJ, 530, L57
- Ryan, S. G., Kajino, T., Beers, T. C., Suzuki, T. K., Romano, D., Matteucci, F., & Rosolankova, K. 2001, ApJ, 549, 55
- Sackmann, I.-J., & Boothroyd, A. I. 1999, ApJ, 510, 217
- Sandner, W., Gallagher, T. F., Safinya, K. A., & Gounand, F. 1981, Phys. Rev. A, 23, 2732



- Sansonetti, C. J., Richou, B., Engelman, Jr. R., & Radziemski, L. J. 1995, *Phys. Rev. A*, 52, 2682
- Savage, B. D., Bohlin, R. C., Drake, J. F., & Budich, W. D. 1977, *ApJ*, 216, 291
- Sembach, K. R., Savage, B. D., Tripp, T. M. 1997, *ApJ*, 480, 216
- Smith, V. V., & Lambert, D. L. 1989, *ApJ*, 345, L75
- Smith, V. V., & Lambert, D. L. 1990, *ApJ*, 361, L69
- Smith, V. V., Lambert, D. L., & Nissen, P. E. 1993, *ApJ*, 408, 262 *ApJ*, 441, 735
- Smith, V. V., Plez, B., Lambert, D. L., & Lubowich, D. A. 1995, *ApJ*, 441, 735
- Snell, R. L., & Vanden Bout, P. A. 1981, *ApJ*, 250, 160
- Snow, T. P., Black, J. H., van Dishoeck, E. F., Burks, G., Crutcher, R. M., Lutz, B. L., Hanson, M. M., & Shuping, R. L. 1996, *ApJ*, 465, 245
- Sofia, U. J., Cardelli, J. A., & Guerin, K. P. 1997, *ApJ*, 482, L105
- Sofia, U. J., Fitzpatrick, E. L., & Meyer, D. M. 1998, *ApJ*, 504, L47
- Sofia, U. J., Meyer, D. M., & Cardelli, J. A. 1999, *ApJ*, 522, L137
- Starrfield, S., Truran, J. W., Sparks, W. M., & Arnould, M. 1978, *ApJ*, 222, 600
- Steigman, G. 1993, *ApJ*, 413, L73
- Suzuki, T. K., Yoshii, Y., & Beers, T. C. 2000, *ApJ*, 540, 99
- Traub, W. A., & Carleton, N. P. 1973, *ApJ*, 184, L11
- Vanden Bout, P. A., Snell, R. L., Vogt, S. S., & Tull, R. G., 1978, *ApJ*, 221, 598
- Vangioni-Flam E., Cassé, M., & Audouze, J. 2000, *Physics Reports*, 333-334, 365
- Vangioni-Flam E., Ramaty, R., Olive, K. A., & Cassé, M. 1998, *A&A*, 337, 714
- Wannier, P., Andersson, B.-G., Penprase, B. E., & Federman, S. R. 1999, *ApJ*, 510, 291
- Wasserburg, G. J., Boothroyd, A. I., & Sackmann, I.-J. 1995, *ApJ*, 447, L37
- Welty, D. E., & Hobbs, L. M. 2001, *ApJS*, 133, 345
- Welty, D. E., Hobbs, L. M., & Kulkarni, V. P. 1994, *ApJ*, 436, 152

White, R. E. 1986, *ApJ*, 307, 777

Wielen, R., Fuchs, B., & Dettbarn, C. 1996, *A&A*, 314, 438

Wielen, R., & Wilson, T.L. 1997, *A&A*, 326, 139

Woosley, S. E., Hartmann, D. H., Hoffman, R. D., & Haxton, W. C. 1990, *ApJ*, 356, 272

Woosley, S. E., & Weaver, T. A. 1995, *ApJS*, 101, 181

Zsargó, J., & Federman, S. R. 2002, *ApJ*, submitted

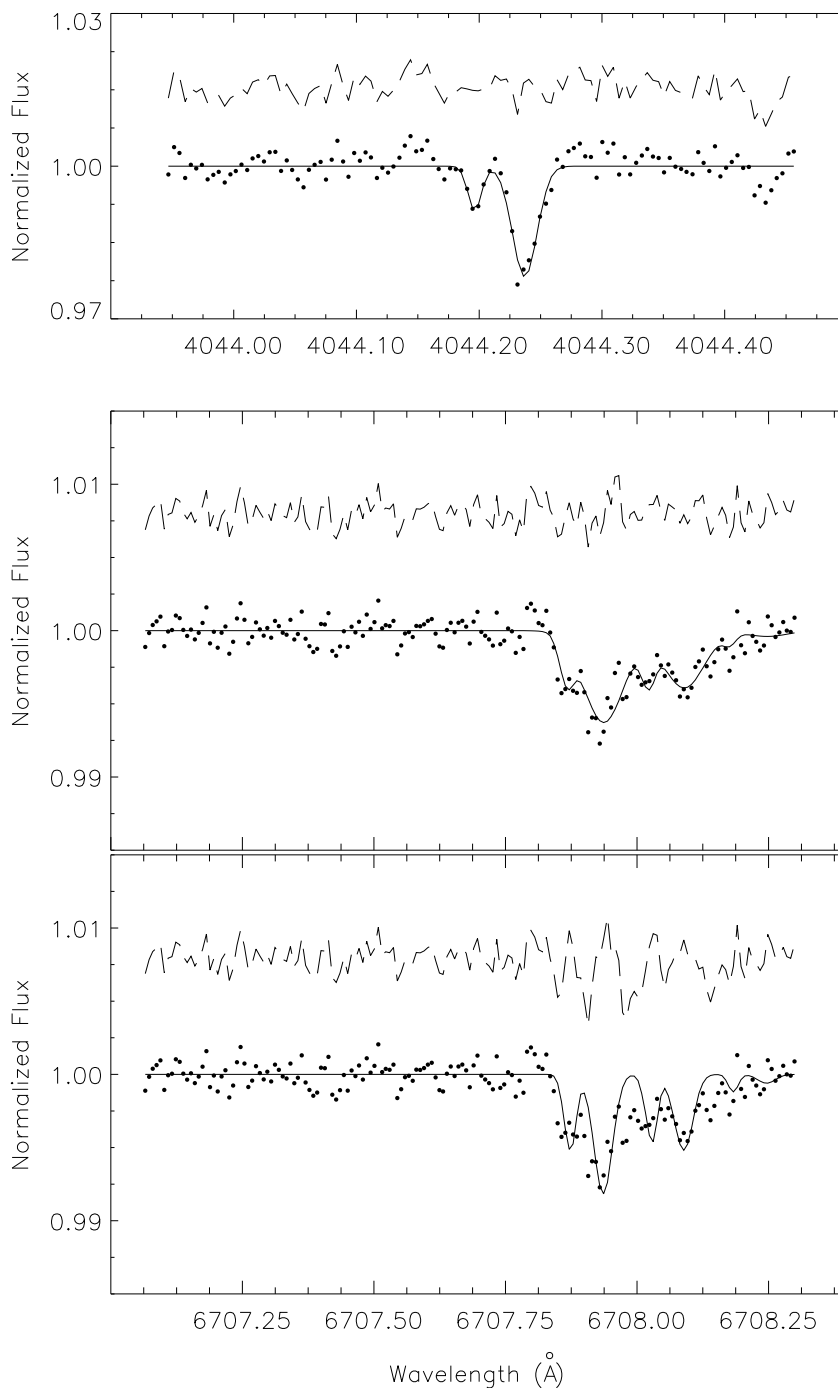


Fig. 1.— *Top*: the preferred two component synthesis of the K I data toward *o* Per using  $b$ -values determined from the line profile. *Middle*: the two component fit of Li I using  $b$ -values determined from  ${}^7\text{Li}$  profile. *Bottom*: velocity structure information from the K I synthesis applied to Li I. In all plots, the data are represented by the filled circles, the fit is the solid line, and the dashed lines are the residuals (data – fit), offset to 1.02 and 1.08 for K I and Li I, respectively.

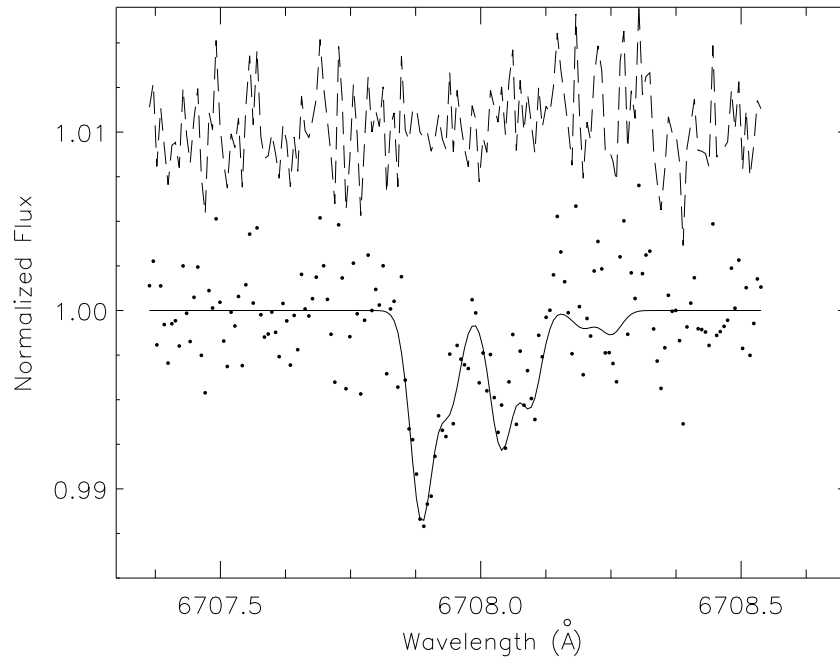


Fig. 2.— The synthesis of the Li I data toward X Per assumes two velocity components (S. R. Federman 2001, private communication). See Figure 1 for a description of the plot. Residuals (data – fit) are offset to 1.01 (dashed line).

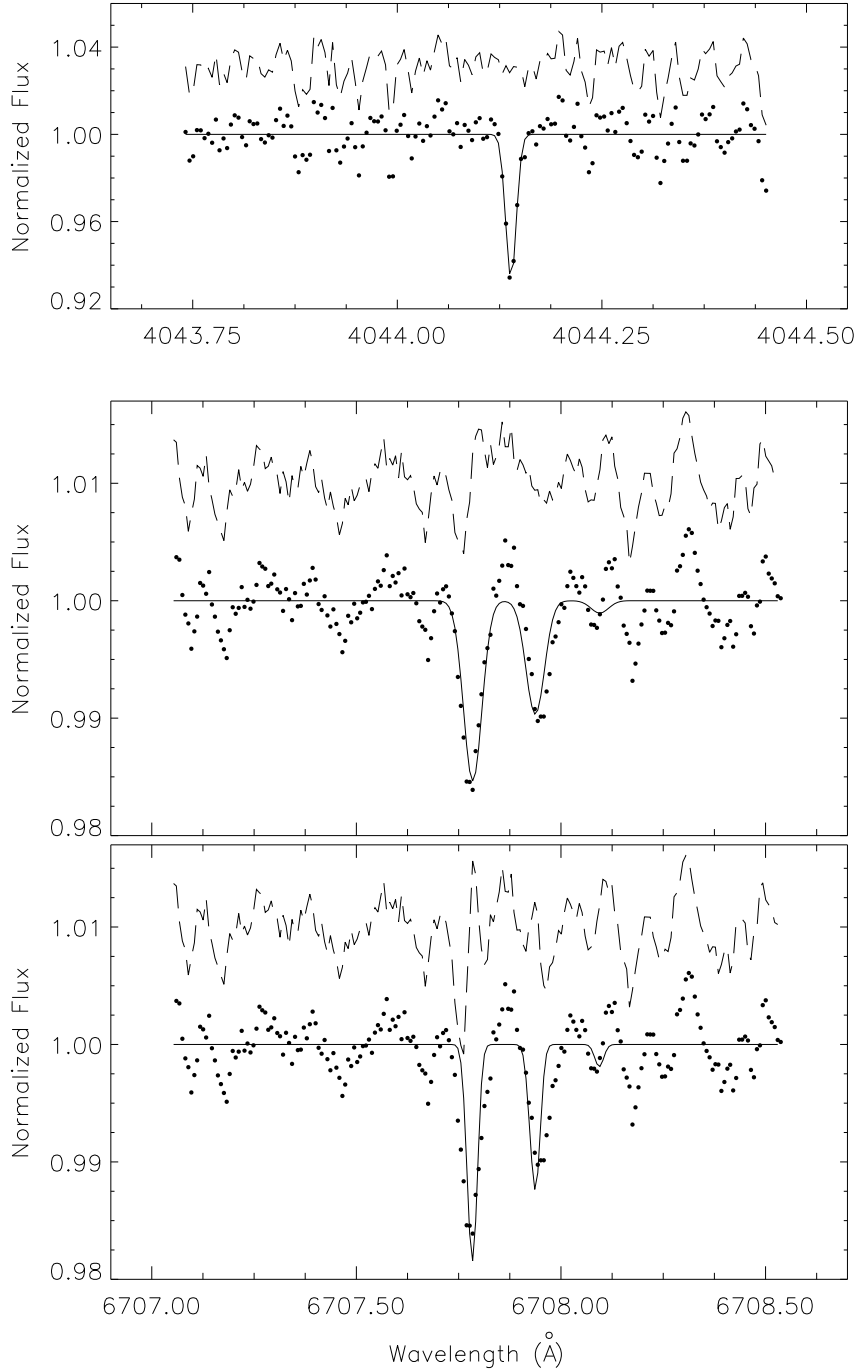


Fig. 3.— *Top*: the one component synthesis of the K I data toward  $\chi$  Oph using  $b$ -values determined from the line profile. *Middle*: one component fit of Li I using  $b$ -values determined from  ${}^7\text{Li}$  profile. The slight disagreement for the weaker  ${}^7\text{Li}$  line with the results of the synthesis is most likely caused by a CCD defect within the level of noise. *Bottom*: fit of Li I using velocity structure information from the K I synthesis. See Figure 1 for a description of the plots. Residuals (dashed lines) for K I and Li I are offset to 1.03 and 1.01, respectively.

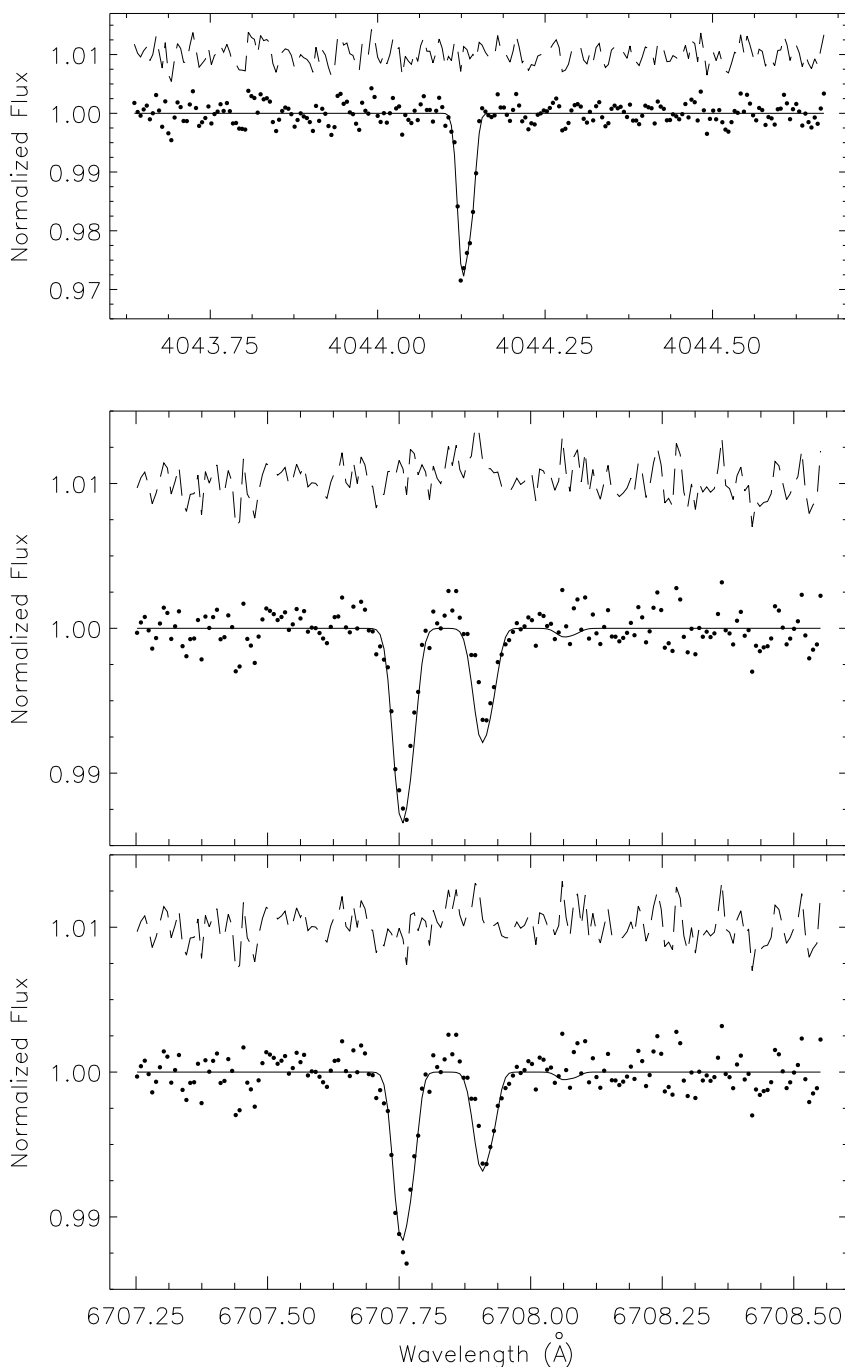


Fig. 4.— *Top*: the preferred two component synthesis of K I using  $b$ -values from UHRs CN observations (Crawford et al. 1994) toward  $\zeta$  Oph. *Middle*: synthesis of Li I using  $b$ -values determined from  ${}^7\text{Li}$  profile. *Bottom*: synthesis of Li I using velocity structure information determined from K I. See Figure 1 for a description of the plots. Residuals (data – fit) are offset to 1.01 (dashed lines) for both K I and Li I.

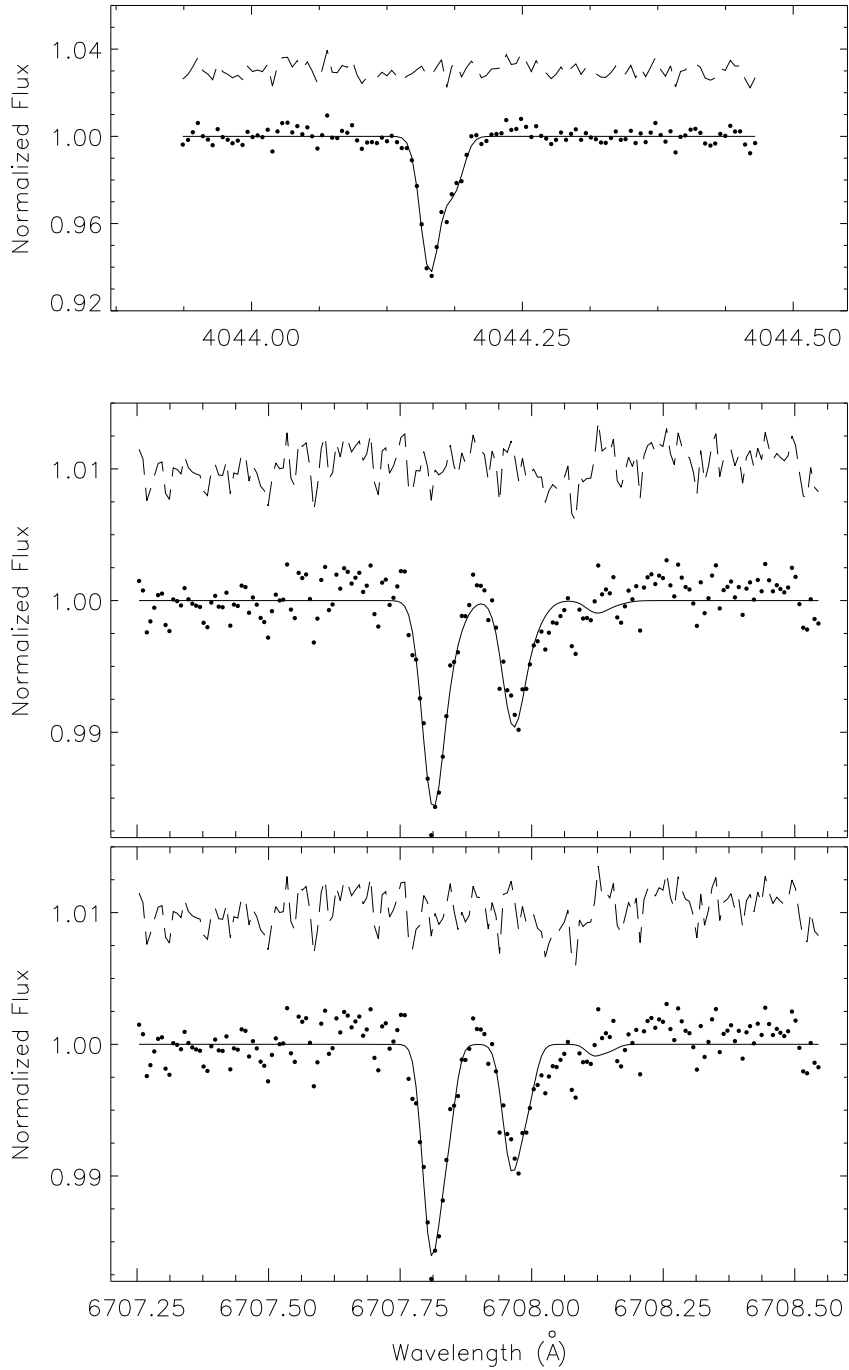


Fig. 5.— *Top*: the two component synthesis of K I toward 20 Aql using  $b$ -values determined from line profile. *Middle*: shows Li I synthesis using  $b$ -values determined from  ${}^7\text{Li}$  profile. *Bottom*: Li I synthesis determined from velocity structure information derived from the K I. See Figure 1 for a description of the plots. Residuals (dashed lines) for K I and Li I are offset to 1.03 and 1.01, respectively.

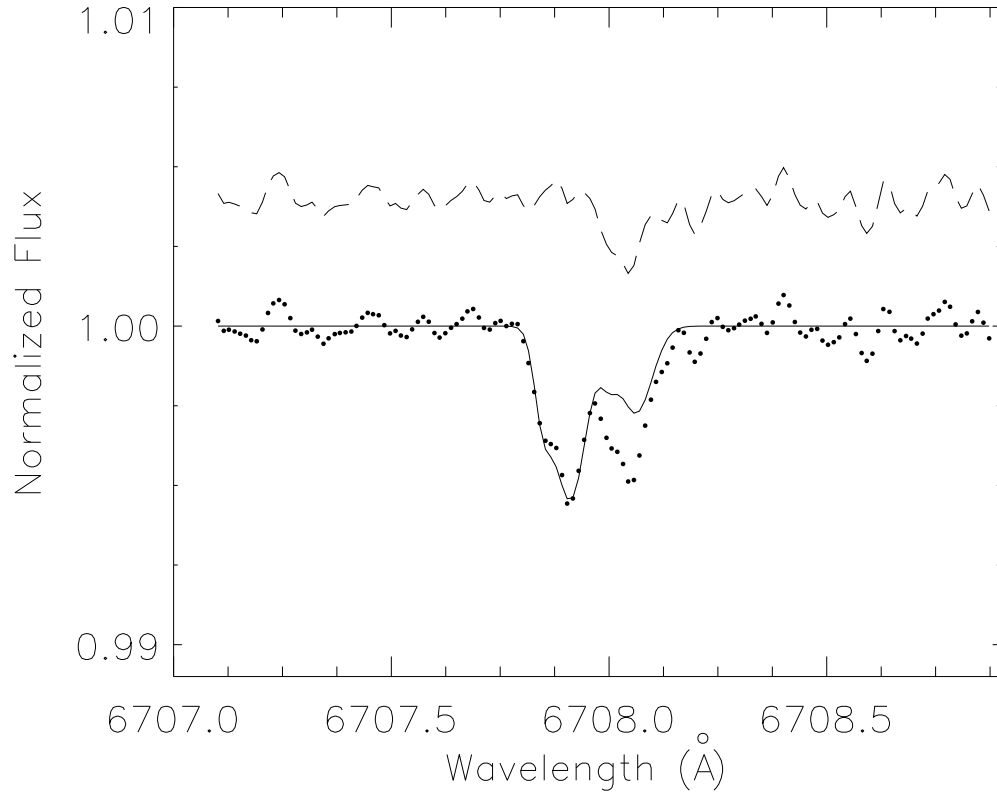


Fig. 6.— We show our previous high-resolution Li I spectrum (Knauth et al. 2000) with a  ${}^7\text{Li}/{}^6\text{Li}$  ratio of 12, as a useful comparison. It is quite clear that a Solar System ratio provides a poor fit to the data toward  $\sigma$  Per. See Figure 1 for a description of the plot. Residuals (data – fit) are offset to 1.04 (dashed line).



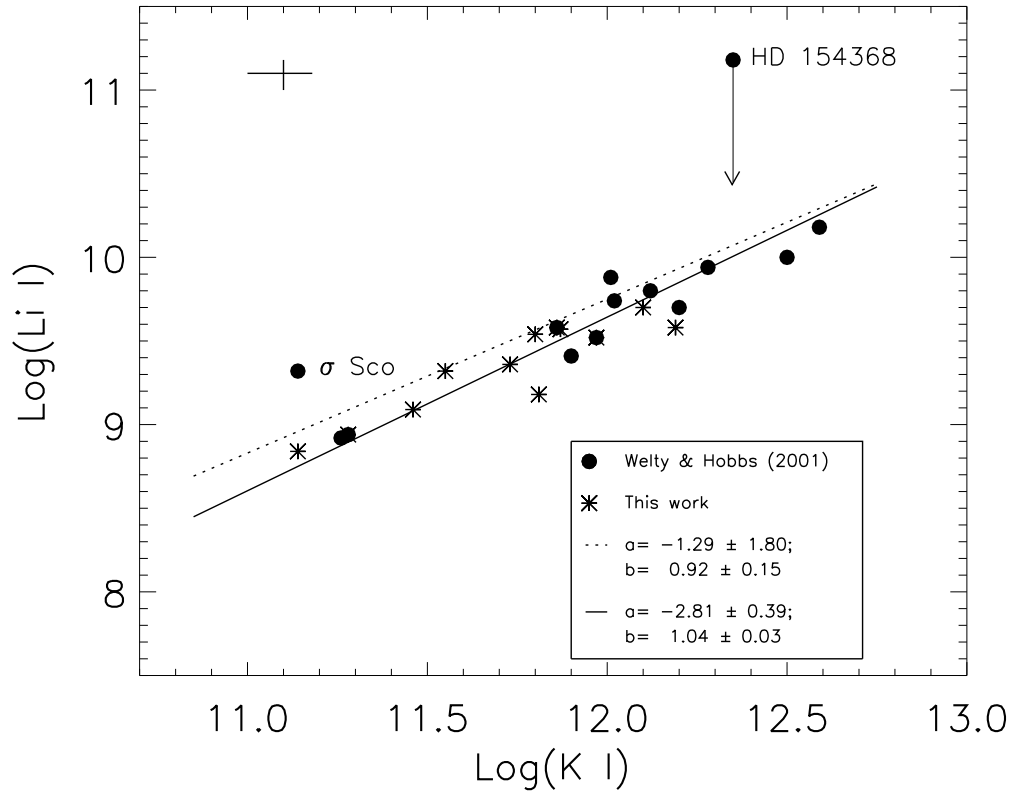


Fig. 7.— Plotted are the values of  $\text{Log}(N(K I))$  vs  $\text{Log}(N(Li I))$  for the lines of sight studied here (asterisks) and from Welty & Hobbs 2001 (filled circles). The dotted line is the best fit from Welty & Hobbs (2001) and the solid line is the least squares fit to all the data. A typical error bar is shown in the upper left of the graph.

Table 1. Stellar Data

Star	Name	Spectral Type <sup>a</sup>	$V^a$ [mag]	$B - V^a$ [mag]	$l^a$ [deg]	$b^a$ [deg]	$d^b$ [pc]	$E(B - V)^c$ [mag]
HD 5394	$\gamma$ Cas	B0 IVe	2.39	-0.10	123.58	-2.15	188	0.14
HD 23180	$\rho$ Per	B1 III	3.86	0.02	160.36	-17.74	453	0.26
HD 22951	40 Per	B0.5 V	4.98	-0.05	158.92	-16.70	283	0.23
HD 24534	X Per	O9.5 V	6.10	0.29	163.08	-17.14	826	0.56
HD36861	$\lambda$ Ori	O8 IIIf	3.39	-0.19	195.05	-12.00	324	0.12
HD 87901	$\alpha$ Leo	B7 V	1.35	-0.11	226.43	48.93	24	...
HD 116658	$\alpha$ Vir	B1 III-IV <sup>+</sup>	1.04	-0.13	316.11	50.84	80	...
HD 148184	$\chi$ Oph	B2 Vne	4.42	0.28	357.93	20.68	150	0.49
HD 149757	$\zeta$ Oph	O9.5 V	2.58	0.02	6.28	23.59	140	0.32
HD 179406	20 Aql	B3 V	5.36	0.09	28.23	-8.31	373	0.33

<sup>a</sup>Simbad database, operated at CDS, Strasbourg, France.

<sup>b</sup>Perryman et al. (1997).

<sup>c</sup>Papaj, Krelowski, & Wegner (1991).

Table 2. Li I and K I Parameters

Species	IP <sup>a</sup> [eV]	$\lambda_{fs}^{b,c}$ [Å]	$f_{fs}^a$	$\lambda_{hfs}^{b,c}$ [Å]	$f_{hfs}^d$
<sup>7</sup> Li I	5.392	6707.764	0.4946	6707.757	0.18550
				6707.769	0.30910
		6707.915	0.2473	6707.908	0.09270
				6707.920	0.15460
<sup>6</sup> Li I	5.392	6707.924	0.4946	6707.922	0.16490
				6707.925	0.32970
		6708.075	0.2474	6708.073	0.08243
				6708.076	0.16490
K I	4.341	4044.143 <sup>a</sup>	0.006089	e	e

<sup>a</sup>Morton (1991).

<sup>b</sup>Sansonetti et al. (1995).

<sup>c</sup> $fs$  – Fine structure,  $hfs$  – Hyperfine structure.

<sup>d</sup>Welty, Kulkarni, & Hobbs (1994).

<sup>e</sup>Hyperfine splitting of K I  $\lambda 4044$  was found to be negligible.

Table 3. UHR Li I and K I Observations

Star	Species	Observatory <sup>a</sup>	Date	Exposure Time [s]	SNR/pixel <sup>b</sup>
$\gamma$ Cas	Li I	McD	08/02/1998 – 08/08/1998	19,200	1000
40 Per	Li I	McD	08/11/1999 – 08/16/1999	14,400	270
		McD	09/15/2000 – 09/21/2000	43,200	470
o Per	Li I	McD	12/30/1998 – 01/05/1999	103,926	720
		McD	12/23/2000 – 12/30/2000	81,827	600
	K I	McD	07/24/1999 – 07/28/1999	7,200	100
		McD	08/11/1999 – 08/16/1999	27,000	290
X Per	Li I	McD	12/23/2000 – 12/30/2000	28,800	200
		McD	12/28/1999 – 12/30/1999	45,000	150
		McD	09/15/2000 – 09/21/2000	75,600	290
$\lambda$ Ori	Li I	McD	12/30/1998 – 01/05/1999	52,200	420
		McD	12/28/1999 – 12/30/1999	21,600	370
$\alpha$ Leo	Li I	McD	12/30/1998 – 01/05/1999	37,800	1050
		McD	12/28/1999 – 12/30/1999	10,800	850
$\alpha$ Vir	K I	McD	12/23/2000 – 12/30/2000	4,500	170
		McD	12/23/2000 – 12/30/2000	12,127	470
		McD	05/11/2000 – 05/13/2000	13,200	320
o Sco	K I	AAO	06/19/1995 – 06/20/1995	2700	130
$\rho$ Oph	K I	AAO	06/19/1995 – 06/20/1995	5700	100
$\chi$ Oph	Li I	AAO	06/19/1995 – 06/20/1995	27900	320
		McD	09/15/2000 – 09/21/2000	9,000	270
	K I	AAO	06/19/1995 – 06/20/1995	5700	160
		McD	05/11/2000 – 05/13/2000	50,400	150
		McD	05/11/2000 – 05/13/2000	50,400	150
$\zeta$ Oph	Li I	AAO	06/10/1994 – 06/12/1994	64800	415
		McD	08/02/1998 – 08/08/1998	13,500	500
		McD	09/15/2000 – 09/21/2000	12,600	430
	K I	AAO	06/19/1995 – 06/20/1995	4800	200
		McD	07/24/1999 – 07/28/1999	44,700	580
HD 154090	K I	AAO	06/19/1995 – 06/20/1995	3600	140
HD 165024	K I	AAO	06/19/1995 – 06/20/1995	2700	160

Table 3—Continued

Star	Species	Observatory <sup>a</sup>	Date	Exposure Time [s]	SNR/pixel <sup>b</sup>
$\mu$ Sgr	K I	AAO	06/19/1995 – 06/20/1995	5800	130
20 Aql	Li I	McD	08/02/1998 – 08/08/1998	51,728	410
		McD	08/11/1999 – 08/16/1999	43,200	410
		McD	09/15/2000 – 09/21/2000	18,000	250
	K I	McD	07/24/1999 – 07/28/1999	32,400	100
		McD	08/11/1999 – 08/16/1999	55,453	200

<sup>a</sup>McD – McDonald Observatory; AAO – Anglo-Australian Observatory.

<sup>b</sup>Final SNR per resolution element from combined binned spectrum: *o* Per – Li I 3040, K I 1050; 40 Per – Li I 1500; X Per – Li I 930;  $\lambda$  Ori – Li I 1440;  $\chi$  Oph – Li I 1130, K I 330;  $\zeta$  Oph – Li I 2600, K I 1500; 20 Aql – Li I 1725, K I 780;  $\gamma$  Cas – Li I 2825;  $\alpha$  Leo – Li I 3675, K I 480;  $\alpha$  Vir – Li I 1330, K I 900.

Table 4. Li I and K I Upper Limits

Star	Species	$W_\lambda$ [mÅ]	$N$ [cm <sup>-2</sup> ]
$\alpha$ Vir	<sup>7</sup> Li I	$\leq 0.11$	$\leq 5.60 \times 10^8$
	K I	$\leq 0.18$	$\leq 2.04 \times 10^{11}$
$\alpha$ Leo	<sup>7</sup> Li I	$\leq 0.05$	$\leq 2.55 \times 10^8$
	K I	$\leq 0.34$	$\leq 3.88 \times 10^{11}$
40 Per	<sup>7</sup> Li I	$\leq 0.11$	$\leq 5.60 \times 10^8$
$\lambda$ Ori	<sup>7</sup> Li I	$\leq 0.11$	$\leq 5.60 \times 10^8$
$\gamma$ Cas	<sup>7</sup> Li I	$\leq 0.07$	$\leq 3.55 \times 10^8$

Table 5. Results of Profile Syntheses

Species	$V_{LSR}^a$ [km s <sup>-1</sup> ]	$b$ -value [km s <sup>-1</sup> ]	$W_\lambda^b$ [mÅ]	$W_\lambda(\text{FIT})$ [mÅ]	$N^c$ [cm <sup>-2</sup> ]	<sup>7</sup> Li/ <sup>6</sup> Li	$\chi^2/\nu$
<i>o</i> Per							
<sup>7</sup> Li I	4.19	0.53	0.12 ± 0.02	0.09 ± 0.02	4.7 ± 1.0		1.28
	7.38	2.53	0.47 ± 0.02	0.60 ± 0.02	30.6 ± 1.1		1.28
<sup>6</sup> Li I	4.19	0.53		0.04 ± 0.02	2.2 ± 1.0	2.1 ± 1.1	1.28
	7.38	2.53		0.08 ± 0.02	3.8 ± 1.0	8.1 ± 2.1	1.28
K I	3.96	0.30	0.14 ± 0.03	0.13 ± 0.03	1.46 ± 0.35		1.80
	6.98	0.92	0.74 ± 0.03	0.78 ± 0.03	8.96 ± 0.35		1.80
<i>X</i> Per							
<sup>7</sup> Li I	5.45	1.20	0.63 ± 0.06	0.63 ± 0.06	32.0 ± 3.1		1.12
	7.85	1.15	0.35 ± 0.06	0.28 ± 0.06	14.2 ± 3.1		1.12
<sup>6</sup> Li I	5.45	1.20		≤ 0.10	≤ 5.1	≥ 6.3	1.12
	7.85	1.15		≤ 0.13	≤ 6.8	≥ 2.1	1.12
<i>χ</i> Oph							
<sup>7</sup> Li I	0.887	1.27	0.93 ± 0.07	0.86 ± 0.07	44.0 ± 4.1		1.30
<sup>6</sup> Li I	0.887	1.27		0.11 ± 0.07	5.8 ± 3.6	7.6 ± 4.8	1.30
K I	-0.30	0.46	1.03 ± 0.10	1.08 ± 0.10	12.7 ± 1.2		1.79
<i>ζ</i> Oph							
<sup>7</sup> Li I	-0.620	0.65	0.41 ± 0.02	0.41 ± 0.02	21.0 ± 1.0		1.81
	0.420	0.57	0.14 ± 0.02	0.22 ± 0.02	11.4 ± 1.0		1.81
<sup>6</sup> Li I	-0.620	0.65		≤ 0.03	≤ 1.8	≥ 11.7	1.81
	0.420	0.57		≤ 0.02	≤ 1.0	≥ 12.0	1.81
K I	-1.25	0.55	0.42 ± 0.03	0.47 ± 0.03	5.36 ± 0.35		3.62
	-0.21	0.45	0.31 ± 0.03	0.25 ± 0.03	2.89 ± 0.34		3.62

Table 5—Continued

Species	$V_{LSR}^a$ [km s <sup>-1</sup> ]	$b$ -value [km s <sup>-1</sup> ]	$W_\lambda^b$ [mÅ]	$W_\lambda(\text{FIT})$ [mÅ]	$N^c$ [cm <sup>-2</sup> ]	<sup>7</sup> Li/ <sup>6</sup> Li	$\chi^2/\nu$
20 Aql							
<sup>7</sup> Li I	2.06	1.06	0.67 ± 0.04	0.67 ± 0.04	34.0 ± 2.1		1.12
	3.35	1.46	0.24 ± 0.04	0.25 ± 0.04	12.8 ± 2.1		1.12
<sup>6</sup> Li I	2.06	1.06		≤ 0.07	≤ 3.6	≥ 9.4	1.12
	3.35	1.46		≤ 0.04	≤ 2.3	≥ 5.6	1.12
K I	1.60	0.75	1.30 ± 0.04	1.34 ± 0.04	15.6 ± 0.5		1.66
	3.21	0.79	0.59 ± 0.04	0.56 ± 0.04	6.40 ± 0.47		1.66

<sup>a</sup>Differences in velocities ( $\sim 0.5$  km s<sup>-1</sup>) between Li I and K I lines, toward the same star, are attributed to uncertainties in using the Li hollow cathode to determine wavelength calibration.

<sup>b</sup>Measured  $W_\lambda$  with 1- $\sigma$  observational uncertainty; No measured  $W_\lambda$  for <sup>6</sup>Li are reported.

<sup>c</sup>Note –  $N(\text{Li I})$  is in units of 10<sup>8</sup> cm<sup>-2</sup> and  $N(\text{K I})$  is in units of 10<sup>11</sup> cm<sup>-2</sup>.



Table 6. Hydrogen and Space Densities

Star	$N(\text{H I})^{\text{a}}$ [ $10^{20} \text{ cm}^{-2}$ ]	$N(\text{H}_2)^{\text{b}}$ [ $10^{20} \text{ cm}^{-2}$ ]	$N_{\text{tot}}(\text{H})^{\text{c}}$ [ $10^{21} \text{ cm}^{-2}$ ]	$n^{\text{d}}$ [ $\text{cm}^{-3}$ ]
40 Per	$11.0 \pm 4.7$	$2.88 \pm 1.23$	$1.68 \pm 1.01$	...
<i>o</i> Per	$6.61 \pm 1.38$	$4.07 \pm 1.44$	$1.48 \pm 0.61$	800
X Per	$5.37 \pm 0.75$	$11.0 \pm 3.0^{\text{e}}$	$2.74 \pm 0.84$	1000
$\lambda$ Ori	$6.03 \pm 2.87$	$0.13 \pm 0.6$	$0.63 \pm 0.42$	...
$\chi$ Oph	$17.0 \pm 3.6$	$4.27 \pm 1.82$	$2.55 \pm 1.21$	400
$\zeta$ Oph	$4.90 \pm 1.14$	$4.47 \pm 1.02$	$1.38 \pm 0.45$	400
20 Aql <sup>f</sup>	$17.0 \pm 2.6$	$6.55 \pm 0.98$	$3.01 \pm 0.64$	850 <sup>g</sup>

<sup>a</sup>Bohlin et al. (1978); Diplas & Savage (1994).

<sup>b</sup>Savage et al. (1977).

<sup>c</sup> $N_{\text{tot}}(\text{H}) = N(\text{H I}) + 2 N(\text{H}_2)$ .

<sup>d</sup>Federman et al. (1994).

<sup>e</sup>Mason et al. (1976).

<sup>f</sup>Hanson et al. (1992); assumes 15% error.

<sup>g</sup>Knauth et al. (2001).

Table 7. Li and K Abundances and Depletion

Star	Li/H	$D(\text{Li})$ [dex]	K/H	$D(\text{K})$ [dex]
<i>o</i> Per	$(2.8 \pm 1.3) \times 10^{-10}$	-0.9	$(2.0 \pm 0.6) \times 10^{-8}$	-0.8
X Per	$(6.3 \pm 2.5) \times 10^{-11}$	-1.5	$(3.3 \pm 1.0) \times 10^{-9}$	-1.6
$\chi$ Oph	$(2.4 \pm 1.3) \times 10^{-10}$	-0.9	$(1.7 \pm 0.8) \times 10^{-8}$	-0.9
$\zeta$ Oph	$(4.0 \pm 1.5) \times 10^{-10}$	-0.7	$(2.6 \pm 0.9) \times 10^{-8}$	-0.7
20 Aql	$(1.5 \pm 0.3) \times 10^{-10}$	-1.2	$(1.7 \pm 0.4) \times 10^{-8}$	-0.9

Table 8. K/Li Abundance Ratios

Star	# of components	$V_{LSR}$ [km s <sup>-1</sup> ]	$N(\text{K})^a$ [10 <sup>11</sup> cm <sup>-2</sup> ]	$N(^7\text{Li} + ^6\text{Li})^a$ [10 <sup>8</sup> cm <sup>-2</sup> ]	$A(\text{K})/A(\text{Li})$
<i>o</i> Per	<b>2</b>	<b>3.96</b>	<b>1.46 ± 0.35</b>	<b>6.90 ± 2.0</b>	<b>58.8 ± 22.1</b>
		<b>6.98</b>	<b>8.96 ± 0.35</b>	<b>34.4 ± 2.1</b>	<b>72.4 ± 5.2</b>
	3	3.96	1.47 ± 0.35	10.8 ± 2.0	38.0 ± 11.5
		6.70	4.41 ± 0.35	12.1 ± 2.0	101.7 ± 18.6
		8.00	2.09 ± 0.35	11.2 ± 2.3	52.1 ± 13.8
	4	4.10	1.47 ± 0.35	10.7 ± 2.0	38.3 ± 11.6
		6.83	4.41 ± 0.35	12.7 ± 2.0	97.2 ± 17.2
		8.12	2.09 ± 0.35	7.6 ± 2.0	76.3 ± 23.7
9.10		0.39 ± 0.08 <sup>b, c</sup>	5.9 ± 2.0	18.5 ± 7.3	
X Per	1	5.85	30.7 ± 2.7	44.2 ± 3.1	195.0 ± 21.9
	<b>2</b>	<b>5.45</b>	<b>7.37 ± 0.22<sup>d</sup></b>	<b>37.1 ± 3.1</b>	<b>55.8 ± 5.0</b>
		<b>7.85</b>	<b>3.53 ± 0.12<sup>d</sup></b>	<b>21.0 ± 3.1</b>	<b>47.2 ± 7.2</b>
	4	4.69	1.70 ± 0.34 <sup>c, d</sup>	10.5 ± 3.1	45.5 ± 16.2
		5.60	4.60 ± 0.92 <sup>c, d</sup>	20.1 ± 3.1	64.2 ± 16.2
		7.47	4.90 ± 0.98 <sup>c, d</sup>	12.9 ± 3.1	106.6 ± 33.3
		8.49	0.18 ± 0.04 <sup>c, d</sup>	7.3 ± 3.1	69.2 ± 32.5
$\chi$ Oph	<b>1</b>	<b>-0.30</b>	<b>12.7 ± 1.2</b>	<b>49.8 ± 7.7</b>	<b>70.7 ± 12.8</b>
$\zeta$ Oph	<b>2</b>	<b>-0.62</b>	<b>5.36 ± 0.35</b>	<b>22.8 ± 1.0</b>	<b>66.0 ± 5.2</b>
		<b>0.42</b>	<b>2.89 ± 0.34</b>	<b>12.4 ± 1.0</b>	<b>65.7 ± 9.4</b>
	3	-0.62	4.09 ± 0.82 <sup>b, c</sup>	19.2 ± 1.1	59.8 ± 12.5
		0.42	2.72 ± 0.54 <sup>b, c</sup>	10.5 ± 1.0	72.8 ± 16.0
		1.65	0.11 ± 0.02 <sup>b, c</sup>	≤ 0.1	≥ 237.5
20 Aql	<b>2</b>	<b>1.60</b>	<b>15.6 ± 0.5</b>	<b>37.6 ± 2.1</b>	<b>115.8 ± 7.5</b>
		<b>3.20</b>	<b>6.40 ± 0.47</b>	<b>15.1 ± 2.1</b>	<b>118.3 ± 18.6</b>

<sup>a</sup>The error is 1- $\sigma$  observational uncertainty.

<sup>b</sup>Welty & Hobbs (2001).

<sup>c</sup>Assumes a 20% uncertainty in measurement.

<sup>d</sup>2 comp. S.R. Federman 2001, private communication; 4 comp. D. Welty 2001, private communication.

Table 9. Molecular Column Densities

Star	$N(\text{CH})$ [ $\text{cm}^{-2}$ ]	$N(\text{C}_2)$ [ $\text{cm}^{-2}$ ]	$N(\text{CN})$ [ $\text{cm}^{-2}$ ]
<i>o</i> Per <sup>a</sup>	$1.3 \times 10^{13}$	$2.7 \times 10^{13}$	$2.6 \times 10^{12}$
40 Per <sup>b</sup>	$1.2 \times 10^{13}$	$3.6 \times 10^{12}$	$6.4 \times 10^{11}$
X Per <sup>a</sup>	$3.1 \times 10^{13}$	$5.3 \times 10^{13}$	$8.4 \times 10^{12}$
$\lambda$ Ori	...	...	...
$\chi$ Oph <sup>a</sup>	$3.4 \times 10^{13}$	$3.5 \times 10^{13}$	$1.3 \times 10^{12}$
$\zeta$ Oph <sup>a</sup>	$2.5 \times 10^{13}$	$1.79 \times 10^{13}$ <sup>c</sup>	$2.6 \times 10^{12}$
20 Aql <sup>d</sup>	$2.0 \times 10^{13}$	$5.2 \times 10^{13}$	$4.2 \times 10^{12}$

<sup>a</sup>Federman et al. (1994).

<sup>b</sup>B.-G. Andersson (2000), private communication.

<sup>c</sup>Lambert, Sheffer, & Federman (1995).

<sup>d</sup>Knauth et al. (2001).

Table 10. Kinetic Temperature and Turbulent Velocity

Star	$T_k^a$ [K]	$v_{turb}^b$ [km s <sup>-1</sup> ]	$v_{turb}^c$ [km s <sup>-1</sup> ]
<i>o</i> Per	98 ± 42 900 <sup>d</sup>	0.16 ± 0.10 0.70 <sup>d</sup>	0.15 ± 0.06 1.20 <sup>d</sup>
X Per <sup>d</sup>	520 788	0.77 0.43	1.05 1.00
χ Oph <sup>d</sup>	220	0.37	0.53
ζ Oph	61 ± 27 63 ± 27	0.37 ± 0.23 0.30 ± 0.18	0.30 ± 0.13 0.21 ± 0.09
20 Aql	287 ± 124 770 ± 330	0.47 ± 0.29 0.39 ± 0.24	0.67 ± 0.29 0.97 ± 0.42

<sup>a</sup> $T_k$  derived from both  $b$ -values.

<sup>b</sup>Uses calculated  $T_k$ .

<sup>c</sup>Assumes  $T_k = 100$  K.

<sup>d</sup>Extreme values of the  $b$ -values ( $\pm 1\text{-}\sigma$ ) were used to arrive at a solution for  $T_k$  and  $v_{turb}$ ; no error bars are given.

Table 11. Constraints on the Stellar  ${}^7\text{Li}$  Source<sup>a</sup>

Star	$({}^7\text{Li}/\text{H})_{ISM}$	$({}^7\text{Li}/\text{H})_{GCR}$	$({}^7\text{Li}/\text{H})_{stars}$
<i>o</i> Per	$(1.8 \pm 0.8) \times 10^{-9}$	$(4.8 \pm 3.3) \times 10^{-10}$	$(1.2 \pm 0.9) \times 10^{-9}$
X Per	$(1.6 \pm 0.8) \times 10^{-9}$	$\leq 6.7 \times 10^{-10}$	$(8.4 \pm 4.8) \times 10^{-10}$
$\chi$ Oph	$(1.8 \pm 0.9) \times 10^{-9}$	$(3.8 \pm 3.5) \times 10^{-10}$	$(1.3 \pm 1.4) \times 10^{-9}$
$\zeta$ Oph	$(1.9 \pm 0.8) \times 10^{-9}$	$\leq 2.6 \times 10^{-10}$	$(1.5 \pm 0.8) \times 10^{-9}$
20 Aql	$(1.8 \pm 0.5) \times 10^{-9}$	$\leq 3.7 \times 10^{-10}$	$(1.3 \pm 0.4) \times 10^{-9}$

<sup>a</sup>Li/H abundance corrected for depletion using our depletion index.